Title: **SREBP governs a triglyceride:glycogen metabolic switch in *Drosophila***

Authors: Rupali Ugrankar-Banerjee[1], Son Tran[3], Sonakshi Srivastava[1], Jade Bowerman[4], Blessy Paul[1], Lauren G. Zacharias[2], Thomas P. Mathews[2], Ralph J. DeBerardinis[2,5], W Mike Henne[1,*]

Affiliations:

[1]Department of Cell Biology, UT Southwestern Medical Center, Dallas, TX 75390

[2]Children's Research Institute (CRI), UT Southwestern Medical Center, Dallas, TX 75390

[3]Perelman School of Medicine, University of Pennsylvania, Philadelphia, PA 19104

[4]Department of Molecular Medicine, Cornell University, Ithaca, NY 14853

[5]Howard Hughes Medical Institute, UT Southwestern Medical Center, Dallas, TX 75390

*for correspondence: mike.henne@utsouthwestern.edu

Abstract:

Tissues store nutrients as triglyceride (TG) or glycogen at specific ratios, but how these reserves are sensed and balanced remains poorly understood. Here we show that blockage of *de novo* lipogenesis (DNL) in the *Drosophila* fat body (FB) triggers a cell autonomous metabolic switch characterized by severe fat depletion and profound glycogen accumulation that supports animal development. Despite lipid loss, *Drosophila* develop normally but exhibit shortened lifespans and impaired female fecundity. Mechanistically, we identify SREBP-dependent metabolic rewiring that facilitates a switch from TG to glycogen storage, triggered by fatty acid deficiency when DNL is inhibited, and which is rescued by dietary fatty acids. Fat depleted FBs require glycolysis but exhibit blunted mitochondrial metabolism, and no dependence on lactate utilization. Finally, we identify histone acetyltransferases (HATs) Nej and Tip60, which support SREBP activity, as essential for this metabolic switch. Collectively, we propose that in response

to DNL deficiency, the fat-depleted FB undergoes a SREBP-mediated TG-to-glycogen metabolic switch preserving organismal development at the cost of reproductive success.

Key findings:

- Fat body-specific FASN1 loss leads to fat-depleted but viable *Drosophila* that complete their developmental lifecycle by rewiring energy metabolism to store glycogen instead of fat
- FASN1-deficient larvae functionally rely on glycogen synthesis and glycolysis, but not lactate metabolism, and display blunted TCA metabolism
- Metabolic screening reveals a SREBP-dependent TG:glycogen metabolic switch in response to blockage of DNL fatty acid biosynthesis
- Histone acetyltransferases (HATs) Nej and Tip60, and acetyl-CoA synthase, are required for the TG:glycogen metabolic switch

Key words:
Fatty acid synthase (FASN); fat body (FB); glycogen; triglyceride (TG); lipid droplet (LD); tricarboxylic acid (TCA) cycle; sterol regulatory element binding protein (SREBP); acetyltransferases (HATs); *de novo* lipogenesis (DNL)

Introduction:

Organisms must sense and allocate nutrients to metabolism, development, and reproduction to maintain homeostasis and populations[1,2]. Dietary carbohydrates are mobilized to glucose and catabolized through glycolysis, the tricarboxylic acid (TCA) cycle, and oxidative phosphorylation to yield carbon dioxide and ATP, the cellular energy currency[3–5]. Excess glucose can be converted into fatty acids and stored as triglycerides (TG) in lipid droplets (LD), or condensed to

glycogen for energy utilization[3,4,6–8]. TG and glycogen reserves are balanced in a tissue and cell-dependent manner, and perturbations in their storage are linked to metabolic disorders including obesity, type 2 diabetes, cardiovascular disease, and cancers[4,5,9–11]. However, the metabolic decision-making that dictates how tissues invest in and balance fat and glycogen stores, and how these reserves are sensed and communicate to ensure cell and organismal homeostasis, remain pervasive questions deeply rooted in understanding and treating metabolic diseases[1].

Drosophila melanogaster is a powerful model to interrogate metabolic imbalance and human metabolic diseases. *Drosophila* encode functional homologs to ~75% of human disease genes, and key metabolic pathways such as insulin and TOR signaling are evolutionarily conserved in flies[10,12,13]. Like humans, *Drosophila* can become obese, lipodystrophic, or diabetic in response to caloric cues or genetic mutations[14–16]. Their primary nutrient storage tissue is the fat body (FB) which shares features of the mammalian adipose tissue and liver[17,18]. In feeding larvae, most dietary carbohydrates are converted to TG and stored in LDs within the FB. Glycogen is also present in the FB at lower concentrations, but its role is not fully clear. Glycogen is quickly mobilized during fasting, and recent studies indicate it may be important for maintaining hemolymph trehalose, the predominant circulating sugar in *Drosophila*, present at ~100-times the level of glucose[12,16,19].

TG stores in the FB are classically thought to support *Drosophila* development as both an energy and biomass resource during pupariation and metamorphosis[20–22], which is characterized by large-scale developmental remodeling[23–25]. However, there is no consensus as to whether FB TG is necessary for this development. Paradoxically, lipodystrophic *Drosophila*, such as the *dLipin* mutant, can survive to the late pharate adult stage, and ~40% become adult flies[26]. Similarly, no lethality is observed for *dSeipin* mutants that exhibit lipid storage and mobilization defects, and adults are viable and fertile[15,27,28]. Studies instead point to the blood-

circulating sugar trehalose as an essential energy source for metamorphosis, raising questions as to how fat and carbohydrate reserves crosstalk and contribute to *Drosophila* development[21,29,30].

TG in the FB is produced from two lipid pools: absorbed lipids from the blood by lipophorin trafficking, or via *de novo* lipogenesis (DNL) that requires fatty acid synthase (FASN)[9,31]. FASN is evolutionarily conserved and catalyzes the synthesis of long chain fatty acids from carbohydrate-derived malonyl-CoA, acetyl-CoA, and the electron donor nicotinamide adenine dinucleotide phosphate (NADPH)[32,33]. *Drosophila* encode three *FASN* genes with distinct tissue expressions. *FASN1/CG3523* is ubiquitously expressed with highest expression in the FB, whereas *FASN2/CG3524* and *FASN3/CG17374* are expressed primarily in the body wall, oenocytes, and hemocytes (*FASN2*) or oenocytes and reproductive system (*FASN3*)[24,34–36]. *Drosophila* hypomorphs for *FASN1* and *FASN2* exhibit reduced larval and adult TG, while null mutants of *FASN1* and *FASN3* display embryonic or early larval developmental arrest[24,34]. Fatty acid synthesis is thus crucial for the generation of energy reserves, cellular membranes, and protection from sugar toxicity[32,35]. However, how FASN-driven lipid synthesis is coordinated with carbohydrate metabolism to enable homeostasis and development remains incompletely understood.

Nutrient reserves must be sensed by cells to maintain energy homeostasis and adapt to nutrient shortages, and alterations in this are drivers of major metabolic diseases and cancers. Key nutrient sensing pathways include the TOR, AMPK, and insulin signaling systems, which monitor carbohydrate, lipid, and amino acids, as well as energy reserves to coordinate organismal development[36–40]. In particular, the sterol regulatory element-binding protein (SREBP) is a conserved transcription factor which promotes lipogenesis and development in *Drosophila* by sensing lipids and responding to cellular fatty acid availability[41–43]. However, how

these different nutrient sensing systems integrate and contribute to TG and glycogen storage in the *Drosophila* FB remains poorly understood. Here we dissect molecular players that orchestrate this TG:glycogen balance by genetically targeting the major fatty acid synthase homolog, FASN1, in the *Drosophila* fat body (FB). We find that blockage of early steps of *de novo* lipogenesis (DNL) in the FB leads to drastic TG loss accompanied by a marked boost in glycogen storage. These fat-depleted *Drosophila* are viable but short-lived, infertile, rely on glycolysis for development, and dampen mitochondrial TCA metabolism. Mechanistically, we identify a SREBP-dependent TG:glycogen switch that mediates this metabolic rewiring and utilization of glycogen as a nutrient reservoir in the absence of fat stores. Further, we reveal specific acetyl-CoA-dependent histone acetyltransferases (HATs) underlying this nutrient rebalancing.

Results:

Fat body specific *FASN1* loss leads to lipid-depleted but viable *Drosophila*

The fat body (FB) is the central metabolic organ in *Drosophila,* and represents much of the larval biomass necessary to achieve metamorphosis[18,20–22]. The FB lipid mass is composed of lipid droplet (LD) triglycerides (TGs), 90% of which is produced from *de novo* lipogenesis (DNL)[9,31,44]. To genetically manipulate these fat stores and study how they influence *Drosophila* development and metabolism, we utilized the FB tissue-specific driver *Dcg-Gal4*[16,45] to selectively RNAi deplete the major *de novo* fatty acyl-CoA synthase *FASN1*, which we previously identified as the major FASN isoform in FB TG synthesis[31] (**Fig 1A, SFig 1A**). FB-specific *FASN1* knockdown (*Dcg-Gal4>FASN1*^{RNAi}, denoted *FASN1*$^{FB\text{-}RNAi}$) yielded larvae that developed in tandem with age-matched controls (we used both *Dcg-Gal4* and *Dcg-Gal4>mCherry*^{RNAi} as controls) and grew to full size (**Fig 1B**). The FB tissue in L3 late feeding/pre-wandering larvae (~100 to 108 h after egg laying, AEL) appeared normal in size, however, FBs appeared translucent instead of the opaque- white typical of fat-engorged tissue

(**Fig 1B, top panel, red arrows-top panel, white arrows-bottom panel**). In line with this, isolated FBs from *FASN1*$^{FB\text{-}RNAi}$ larvae sank in PBS buffer, indicating they lost buoyancy normally provided by lipids (**SFig 1B**). This was not due to altered cell size or morphology, as larval FBs contained typical but slightly larger adipocytes, indicating tissue development was not affected by FASN1 knockdown (KD) (**Fig 1C,D**).

To determine how FASN1 deficiency impacted LDs in the FB, we conducted z-section confocal imaging of FBs excised from larvae. *FASN1*$^{FB\text{-}RNAi}$ FBs displayed a near complete lack of large LDs normally visible in the tissue mid-plane (mid-plane LDs, or mLDs) that constitute the bulk of TG stores in FB cells[46]. However, *FASN1*$^{FB\text{-}RNAi}$ FBs did exhibit small peripheral LDs (pLDs) at the tissue surface, consistent with previous work indicating these pLDs are largely independent of DNL, and may be generated from extracellular lipids delivered to the FB[31] (**Fig 1E,F**). pLDs near the cell surface were also observed by transmission electron microscopy (TEM) (**Fig 1G, pLDs at red arrows**). In contrast, most of the *FASN1*$^{FB\text{-}RNAi}$ FB cell cytoplasm was devoid of mLDs, appearing vacant. As expected, total larval TG was significantly reduced by ~85% in *FASN1* KD compared to controls (**Fig 1H**). As expected, FB-RNAi KD of *FASN3*, or a global mutation of *FASN2*, did not similarly deplete FB LD stores, as these *FASN* isoforms do not play major roles in the FB[46] (**SFig 1C, see Table S1 for list of *Drosophila* stocks**).

Perturbations in FB fat storage can cause ectopic lipid accumulation in other tissues such as the mid-gut[47], however gut TG levels were 50% lower in *FASN1*$^{FB\text{-}RNAi}$ larvae relative to controls (**SFig 1D**). To validate the *FASN1*$^{FB\text{-}RNAi}$ phenotype, we targeted FASN1 using additional FB drivers, *Cg-Gal4* and *r4-Gal4*, which also resulted in LD depletion similar to Dcg-Gal4 (**SFig 1E**). Since lipogenesis is essential to protect the animal from glucotoxicity[16,18] we also examined how the disruption of dietary carbohydrate-to-fat conversion in *FASN1*$^{FB\text{-}RNAi}$ larvae impacted hemolymph glucose and trehalose. We measured these in control and *FASN1*$^{FB\text{-}RNAi}$ pre-

wandering L3 larvae. Notably, circulating glucose levels were not significantly altered, but total circulating carbohydrates comprised primarily of trehalose were substantially up in *FASN1*$^{FB\text{-}RNAi}$ larvae, suggesting they were hypertrehalosemic (**SFig 1F,G**). Strikingly, despite their dramatic TG loss and elevated circulating carbohydrates consistent with a 'diabetic state'[16], *FASN1*$^{FB\text{-}RNAi}$ larvae appeared healthy and progressed to pupation with no notable developmental delay or impact on pupal size (**Fig 1I**). Collectively, this indicates that *FASN1*$^{FB\text{-}RNAi}$ *Drosophila* larvae, despite lacking a majority of their FB TG stores, are still able to achieve the critical weight required for pupation and metamorphosis.

FASN1$^{FB\text{-}RNAi}$ **flies are viable but exhibit shortened lifespan, starvation sensitivity, and reduced fecundity**

Remarkably, *FASN1*$^{FB\text{-}RNAi}$ pupae complete metamorphosis and emerge as normal sized adult *Drosophila*, with weights comparable to control flies (**Fig 2A,B**). As expected, *FASN1*$^{FB\text{-}RNAi}$ female and male flies have virtually undetectable TG (**Fig 2C**). Given this dramatic fat deficiency, we investigated how this influenced *FASN1*$^{FB\text{-}RNAi}$ fly lifespan and metabolic stress responses. We found *FASN1*$^{FB\text{-}RNAi}$ flies of both sexes displayed significantly shortened median lifespan on standard food (**Fig 2D**). Moreover, *FASN1*$^{FB\text{-}RNAi}$ adults died roughly twice as quickly when maintained on water but no food source, indicating starvation sensitivity consistent with a lack of TG reserves (**Fig 2E**).

As nutrient reserves are tightly linked with reproductive success[48,49], we next examined how DNL blockage in the FB impacted fecundity by monitoring whether *FASN1*$^{FB\text{-}RNAi}$ female and male flies could successfully generate progeny. Indeed, eggs deposited by control (*Dcg-Gal4)* females mated with *FASN1*$^{FB\text{-}RNAi}$ males showed slightly decreased viability relative to those from *Dcg-Gal4* fathers, suggesting *FASN1* loss in the male FB mildly perturbed fecundity (**Fig**

2F). Strikingly, *FASN1*$^{FB\text{-}RNAi}$ females mated with either control or *FASN1*$^{FB\text{-}RNAi}$ males failed to lay eggs, indicating *FASN1*$^{FB\text{-}RNAi}$ females exhibited substantial infertility (**Fig 2F**).

The *Drosophila* female fly reproductive system consists of two ovaries, each with 20-30 ovarioles. An ovariole is organized into a procession of egg chambers. Within these chambers, a single nurse cell will become an oocyte, which matures through 14 morphologically distinct stages during oogenesis[50,51]. Dissection of the internal reproductive organs of *FASN1*$^{FB\text{-}RNAi}$ females revealed shrunken and underdeveloped ovaries that did not produce mature oocytes (**Fig 2G, SFig 2A, oocytes in SFig 2A denoted by white arrows**). Close examination revealed *FASN1*$^{FB\text{-}RNAi}$ egg chambers arrested at stage 9-10, when follicle cells normally migrate to surround the oocyte (**Fig 2H, follicle cells denoted by yellow arrows, oocyte by white arrows**). In control ovaries, lipid droplets accumulated in nurse cells (**Fig 2I, denoted by orange arrows**) and were subsequently transferred to the growing oocyte (**Fig 2I, denoted by purple arrow**). In contrast, *FASN1*$^{FB\text{-}RNAi}$ egg chambers were largely devoid of lipid droplets, consistent with reports their deficiency correlates with defective oogenesis[50–53]. Failure to pass this key metabolic checkpoint in oocyte maturation likely resulted in degeneration of the egg chambers, as no discernable cells with nuclear DAPI staining were visible in the interior of *FASN1*$^{FB\text{-}RNAi}$ ovaries (**SFig 2B, blue arrows).** Collectively, this indicates that while FASN1-dependent DNL in the FB is dispensable for animal development, FASN1 depletion compromises lifespan, starvation resistance, and female fecundity.

FASN1-deficient *Drosophila* FBs metabolically rely on glycogen storage for development

The fact that DNL blockage in the FB led to viable but largely TG-depleted *Drosophila* provided a unique opportunity to dissect how adipose metabolism is rewired to support animal development in such conditions. *Drosophila* FB lipids are proposed to play crucial roles in development, serving as an energy source for metamorphosis, biomaterials for growth, and a

metabolic buffer to counter caloric overload[10,22,24]. Given this, we investigated what proteins and pathways were necessary for metamorphosis in *FASN1*$^{FB\text{-}RNAi}$ animals. We conducted unbiased global liquid chromatography tandem mass spectrometry (LC-MS) proteomics of isolated FBs from control and *FASN1*$^{FB\text{-}RNAi}$ pre-wandering L3 larvae. Principal component analysis (PCA) revealed control and *FASN1*$^{FB\text{-}RNAi}$ FBs exhibited substantial differences in the relative abundances of many proteins (**Fig 3A, Table S2**). Proteomics also confirmed efficient *FASN1* KD, as FASN1 was among the most strongly downregulated proteins in *FASN1*$^{FB\text{-}RNAi}$ FBs (**Fig 3B**). We also noted reduced abundances of proteins important for TG synthesis or storage, such as glycerol kinase Gk1, perilipins Lsd-1 and Lsd-2, proteins involved in TG breakdown such as Bmm (mammalian ATGL homolog), pdgy and CPT2 (involved in fatty acid β-oxidation) (**Fig 3B**). As expected, GO term pathway analysis revealed lipid metabolic processes, particularly those related to fatty acid, TG biosynthesis, and fatty acid catabolism, were among the most decreased in *FASN1*$^{FB\text{-}RNAi}$ FBs (**Fig 3C**).

Whereas lipid metabolism appeared blunted in *FASN1*$^{FB\text{-}RNAi}$ FBs, interestingly GO term analysis indicated carbohydrate catabolic and glycolytic processes were among the most upregulated (**Fig 3D**). Consistent with increased glycolysis, protein levels of Glo1, a key detoxication enzyme that degrades the toxic glycolysis biproduct methylglyoxal, was elevated (**SFig 1C**)[35]. Also among the most elevated carbohydrate-related proteins was target-of-brain-insulin (tobi), which was only detected in *FASN1*$^{FB\text{-}RNAi}$ FBs (**Fig 3B, green box**), and whose mRNA level increased ~8-fold in *FASN1*$^{FB\text{-}RNAi}$ FBs compared to controls (**Fig 3E).** Tobi is a conserved alpha-glucosidase expressed primarily in FB and gut, and is activated during sugar mobilization[54,55]. Alpha-glucosidases like tobi are speculated to contribute to glycogen breakdown. Therefore, we examined FB glycogen levels in control and *FASN1*$^{FB\text{-}RNAi}$ FBs. Strikingly, periodic acid-Schiff (PAS) staining revealed significantly elevated glycogen in *FASN1*$^{FB\text{-}RNAi}$ FBs compared to controls, and biochemical measurements confirmed a remarkable ~20-fold glycogen increase in

FASN1$^{FB\text{-}RNAi}$ FBs (**Fig 3F,G).** Increased glycogen granules were also detected in *FASN1*$^{FB\text{-}RNAi}$ FBs by imaging *Glycogenin-YFP,* which stimulates glycogen polymerization[56] (**SFig 3A**). QPCR revealed induction of other key enzymes involved in glycogen synthesis (glycogenesis) and glycogen breakdown (glycogenolysis); in particular glycogen phosphorylase (GlyP) is attributed to glycogen breakdown in the *Drosophila* FB[57] (**SFig 3B**). This suggested that in the absence of fat stores, larvae channel nutrients into FB glycogen for energy storage and utilization. From this, we hypothesized that *FASN1*$^{FB\text{-}RNAi}$ larvae depended on carbohydrate metabolism for development.

To test this, we RNAi depleted the glycogen synthesis enzyme GlyS, or the putative alpha-glucosidase tobi, either alone or in combination with *FASN1* specifically in the FB. Whereas RNAi loss of GlyS or tobi alone did not impact larval development into flies, loss of either in combination with *FASN1*$^{FB\text{-}RNAi}$ led to developmental arrest during the pupal stage (**Fig 3H,I**). Next, we determined whether *FASN1*$^{FB\text{-}RNAi}$ larvae mobilized glycogen during larval and pupal development. We observed glycogen levels in *FASN1*$^{FB\text{-}RNAi}$ animals declined rapidly compared to controls during the transition from late feeding larvae to pharate adults **(SFig 3D,E**). In fact, *FASN1*$^{FB\text{-}RNAi}$ pharate adults contained only ~15% of their initial glycogen stores, consistent with glycogen mobilization to support development. In contrast, glycogen levels in controls remained steady through metamorphosis while there was a pronounced decline in TG. A small dip in TG levels of *FASN1*$^{FB\text{-}RNAi}$ was also observed, however, the energy available through TG lipolysis in this fat-deficient animal is likely negligible (**SFig 3D,E)**. Furthermore, whole adult fly glycogen was lower in both male and female *FASN1*$^{FB\text{-}RNAi}$ flies compared to controls, consistent with the utilization of larval fat body glycogen during metamorphosis, as well as the absence of a discernible adult fat body in *FASN1*$^{FB\text{-}RNAi}$ flies. (**SFig 3F**). Collectively, this indicates *FASN1*$^{FB\text{-}RNAi}$ larvae exhibit significantly boosted carbohydrate storage in the form of FB glycogen, and functionally require glycogen synthesis and breakdown for development.

FASN1$^{FB\text{-}RNAi}$ **larvae boost glycolysis and blunt mitochondrial metabolism**

Given that *FASN1$^{FB\text{-}RNAi}$* larvae elevate glycogen storage and utilization, we hypothesized they rely on glycolysis for development. Indeed, proteomics of larval FBs revealed glycolysis enzymes including Hex-A, Pgi, Pfk, Gapdh2, Eno, and Pyk (pyruvate kinase) were significantly more abundant in *FASN1$^{FB\text{-}RNAi}$* FBs compared to controls (**Fig 4A,B**). Transcript analysis also showed increased mRNA for *Pyk* which generates the glycolytic end-product pyruvate (**SFig 4A**). To confirm pyruvate levels were boosted in *FASN1$^{FB\text{-}RNAi}$* larval FBs, we expressed the fluorescent pyruvate biosensor *UAS-mito-PyronicSF*[58] in the FB. Indeed, PyronicSF was substantially brighter in *FASN1$^{FB\text{-}RNAi}$* FBs compared to controls, indicating elevated pyruvate production (**Fig 4C**). We also queried whether Pyk was required for *Drosophila* development in *FASN1$^{FB\text{-}RNAi}$* animals by depleting *PyK* either alone or in combination with *FASN1* in the FB. Strikingly, whereas *PyK* loss alone did not impact *Drosophila* development into flies, *FASN1* and *PyK* dual loss led to ~75% pupal arrest and subsequent death (**Fig 4D**). This indicated PyK was important for *Drosophila* development when FASN1 was depleted, suggesting increased need for glycolysis.

Pyruvate is transported to the mitochondrial matrix where it is converted into acetyl-CoA and subsequently catabolized by the mitochondrial tricarboxylic acid (TCA) cycle and electron transport chain (ETC) to generate energy. During hypoxic conditions, pyruvate remains in the cytosol and is converted to lactate and ATP is produced through anaerobic glycolysis only. This pathway is often upregulated in cancer cells, even in the presence of oxygen, in the so-called Warburg effect[2,59,60]. To determine whether *FASN1$^{FB\text{-}RNAi}$* FBs relied on TCA or lactate metabolism for bioenergetics, we measured mRNA levels of enzymes that catalyze production of acetyl-CoA and lactate. Pdha, the catalytic subunit of the pyruvate dehydrogenase complex responsible for acetyl-CoA production, was moderately upregulated, while its negative regulator

Pdk was downregulated in *FASN1*$^{FB\text{-}RNAi}$ FBs (**Fig 4A, SFig 4A**). Further, we found transcripts of lactate dehydrogenase (*Ldh*), which converts pyruvate to lactate, were downregulated with FASN1 loss (**SFig 4A**). To functionally assess if lactate production was necessary to fuel *FASN1*$^{FB\text{-}RNAi}$ animal development, we RNAi depleted *Ldh* in the FB either alone or in combination with *FASN1*. In both cases *Drosophila* development into flies was not substantially impacted, indicating lactate production was not functionally required for development (**Fig 4E**). Collectively, this indicates that *FASN1*$^{FB\text{-}RNAi}$ larvae elevate glycolysis and promote conversion of pyruvate to acetyl-CoA, but may not require lactate for development.

Acetyl-CoA derived from pyruvate can be partitioned to DNL or the TCA cycle, which generates metabolic intermediates for bioenergetics and other cellular processes[4,5]. Given that FASN1 depletion blocks DNL, acetyl-CoA could be channeled into the TCA cycle, resulting in increased TCA activity. Surprisingly however, proteomics indicated lower expression of most TCA enzymes in *FASN1*$^{FB\text{-}RNAi}$ larval FBs compared to controls (**Fig 4F**). Notably, both protein and mRNA levels for Idh (isocitrate dehydrogenase), the TCA rate limiting enzyme[61,62], were decreased in *FASN1*$^{FB\text{-}RNAi}$ FBs, suggesting TCA metabolism was not boosted and may in fact be blunted (**SFig 4B**). Consistent with this, both mRNA and protein levels of ATP citrate lyase (ATPCL), a cataplerotic enzyme that shunts citrate out of the TCA cycle[58], were significantly increased in *FASN1*$^{FB\text{-}RNAi}$ FBs (**Fig 4G)**, suggesting that DNL blockage may dampen TCA activity. Furthermore, proteomics showed slight downregulation of mitochondrial electron transport chain (ETC) proteins involved in oxidative phosphorylation (OXPHOS) in *FASN1*$^{FB\text{-}RNAi}$ FBs (**SFig 4C**). Similarly, proteins involved in mitochondrial fatty acid oxidation (FAO) decreased in abundance in *FASN1*$^{FB\text{-}RNAi}$ FBs, indicating more general dampening of mitochondrial metabolism (**SFig 4D**). Consistent with these metabolic changes, mitochondria in

FASN1$^{FB\text{-}RNAi}$ FBs stained with MitoSOX had lower signal intensity relative to controls, suggesting lower mitochondrial activity (**Fig 4H,I**).

To more comprehensively understand how DNL blockage influenced FB mitochondrial metabolism, we conducted LC-MS/MS metabolomic profiling of isolated FBs. Metabolomics suggested altered mitochondrial metabolism, and *FASN1*$^{FB\text{-}RNAi}$ FBs displayed elevated TCA metabolites including malate, succinate, and alpha-ketoglutarate (**Fig 4J, Table S3**). Indeed, previous reports show that impaired TCA enzyme activity can result in buildup of these and other TCA intermediates[61,63,64]. Additionally, metabolomics revealed substantially reduced long-chain acylcarnitines compared to control FBs, further suggesting attenuated FAO activity (**Fig 4J**). Taken together, this suggests *FASN1*$^{FB\text{-}RNAi}$ larval FBs require glycolysis to fuel development but may repress mitochondrial metabolic pathways including TCA and FAO, and do not rely on TCA metabolism for fly development.

A cell autonomous TG:glycogen metabolic switch is triggered specifically by early stage DNL blockage

Blocking DNL in the FB significantly boosted glycogen storage and increased reliance on glycolysis, consistent with a TG:glycogen metabolic switch that preserved organismal development in the absence of fat stores. To mechanistically investigate how this metabolic switch was initiated (and whether it was a general consequence of impaired lipid biosynthesis), we examined whether disruption of distinct steps within the DNL pathway could produce a similar effect. First, we RNAi depleted acetyl-CoA carboxylase (ACC), the rate limiting enzyme of DNL, immediately upstream of FASN1. As expected, this also triggered LD depletion in the FB akin to *FASN1*$^{FB\text{-}RNAi}$, and importantly a comparable boost of glycogen stores was also observed (**Fig 5A,C, SFig 5A**).

In contrast, FB-specific depletion of enzymes downstream of FASN1 in the DNL pathway including acyl-CoA ligase ACSL, the acyltransferase GPAT4, dLipin, and triglyceride synthesis enzyme Midway (Mdy) did not boost glycogen. In fact, in each of these knockdowns glycogen levels resembled control levels or were even slightly lower (**Fig 5A,C**). Of note, several of these RNAi lines resulted in significant LD loss such as *dLipin*$^{FB\text{-}RNAi}$, previously reported as lipodystrophic[26], but despite this *dLipin*$^{FB\text{-}RNAi}$ did not accumulate excess glycogen (**Fig 5A,C**,**SFig 5A)**. This suggested the TG:glycogen metabolic switch that boosted glycogen storage was triggered specifically by blockage of *early steps* in the DNL pathway, possibly due to loss of fatty acid synthesis itself, rather than general perturbation of lipid biosynthesis. In support of this, FB-targeted RNAi depletion of other factors known to diminish LD stores[65,66] (Act5C, Ck1alpha, Uba1), also did not display increased glycogen storage (**Fig 5B,D, SFig 5B**). In fact, Act5C and Ck1alpha depletion reduced glycogen compared to controls (**Fig 5B,D**). This collectively suggested that boosted FB glycogen storage was not simply a consequence of depleting LD lipid stores, but rather dependent on blockage of early stage DNL.

To understand if this TG:glycogen switch was cell autonomous, we utilized the ubiquitous but mosaic driver *da-Gal4* that activates a *UAS-RNAi* transgene in a subset of FB cells[65]. Indeed, *da-Gal4>FASN1*^{RNAi} larval FBs exhibited a mosaic pattern of LD-depleted cells adjacent to lipid engorged cells (**Fig 5E, top panel**). In line with this, PAS stained *da-Gal4>FASN1*^{RNAi} FBs exhibited a similar mosaic pattern for glycogen stain, with only *FASN1-KD* cells darkened by high glycogen (**Fig 5E', bottom panel, white arrows**) while nearby unaffected cells resembled controls (**Fig 5E, light blue arrows**). This indicated the TG:glycogen metabolic switch was a cell autonomous effect of DNL blockage.

ACC and FASN1 are early players in lipid biosynthesis and generate *de novo* fatty acids, whereas downstream DNL enzymes modify fatty acyl-CoAs into lyso-lipids and mature lipids for

the cell[34,67]. As such, we hypothesized that fatty acids themselves may regulate the TG:glycogen metabolic switch in the FB. Palmitic acid is the major enzymatic product of FASN1, so we tested if supplementing dietary PA to *FASN1*$^{FB\text{-}RNAi}$ animals suppressed the TG:glycogen metabolic switch. We supplemented the *Drosophila* diet with palm oil (PO), which is composed of ~44% PA [68]. Strikingly, *FASN1*$^{FB\text{-}RNAi}$ larvae cultured in 10% PO food now displayed normal glycogen levels resembling control larvae, suggesting PO addition suppressed the metabolic switch (**Fig 5F,G)**. As expected, *FASN1*$^{FB\text{-}RNAi}$ larvae fed 10% PO also displayed increased LD stores (**SFig 5C**). Notably, even control animals on 10% PO diets had visibly larger LDs, and glycogen amounts in these animals were reduced by ~25%, further suggesting a tradeoff between TG and glycogen levels (**Fig 5F,G, SFig 5C**). These findings indicate that fatty acids are sufficient to modulate TG:glycogen levels, and support the model that inhibition of fatty acid biosynthesis, rather than lipid or TG depletion, may drive the TG:glycogen metabolic switch boosting FB glycogen storage.

A Periodic Acid-Schiff (PAS) glycogen screen reveals SREBP as a regulator of the TG:glycogen metabolic switch

Since blocking fatty acid synthesis appeared critical for boosting glycogen storage in *FASN1*$^{FB\text{-}RNAi}$ FBs, we hypothesized lipid sensing factors mediate this metabolic rewiring. To identify these factors, we performed a candidate-based screen targeting nutrient-sensing pathways. These included insulin signaling components, Akh (the *Drosophila* glucagon analog), target-of-rapamycin (TOR), AMPK pathway factors, glycogen regulators, SREBP (a major lipid metabolism transcription factor), and genes related to glycolysis or other metabolism[39,69–74]. In total, we crossed over 60 RNAi or gain-of-function UAS lines to the FB-specific *Dcg-Gal4* driver, either alone or in combination with *FASN1*-RNAi. Larval fat bodies were analyzed by PAS

staining to assess glycogen levels and to identify modifiers that suppressed glycogen accumulation in FASN1-deficient animals.

Notably, hyperactivation of AMPK signaling via a *UAS-AMPK* transgene did not alter glycogen levels compared to controls (**Fig S6A,B)**. Moreover, *UAS-AMPK* over-expression in *FASN1*$^{FB\text{-}RNAi}$ failed to alleviate glycogen accumulation caused by *FASN1* loss, suggesting AMPK signaling was not involved in the TG:glycogen switch. Next, we tested how perturbation of glycolysis flux and downstream metabolites impacted glycogen, since metabolites can provide negative feedback to carbohydrate metabolism. For example, although glycolytic proteins are upregulated in *FASN1*$^{FB\text{-}RNAi}$ (**Fig 4B**), metabolomics showed that citrate accumulated in these cells, potentially due to blunted TCA metabolism (**Fig 4J, SFig 6C**). Citrate is an allosteric inhibitor of phosphofructokinase (Pfk), a key regulatory "pacemaker" glycolysis enzyme that can alter the distribution of glycolytic intermediates without affecting the total flux[75]. Interestingly Pfk depletion alone significantly boosted glycogen, mirroring FASN1 loss (**SFig 6 D,E**); indeed Pfk deficiency has been linked to human glycogen storage disease type VII[76]. To test whether Pfk and citrate influenced the TG:glycogen metabolic switch, we overexpressed *UAS-Pfk* and RNAi-targeted the major citrate synthase enzyme kdn, and determined whether these could attenuate glycogen accumulation in *FASN1*$^{FB\text{-}RNAi}$ FBs. Neither Pfk overexpression nor kdn loss significantly altered glycogen levels either alone or with FASN1 depletion **(Fig 6A,B**). Collectively, this suggests neither AMPK signaling nor alterations in Pfk or glycolysis are drivers of the TG:glycogen metabolic switch.

We next examined insulin signaling, given its well established role in glycogen synthesis during feeding and development[37,70]. As expected, we found that dampening insulin signaling via RNAi depletion of the insulin receptor in the FB (*InR*$^{FB\text{-}RNAi}$) reduced FB glycogen stores (**Fig 6C,D**). Notably, *InR*$^{FB\text{-}RNAi}$ combined with *FASN1*$^{FB\text{-}RNAi}$ led to a moderate but statistically significant

glycogen reduction compared to *FASN1*$^{FB\text{-}RNAi}$ alone (**Fig 6C,D**). Since TOR signaling is downstream of insulin signaling[36,37], we also RNAi depleted *Drosophila* TOR (*TOR*$^{FB\text{-}RNAi}$), and found this alone also decreased FB glycogen. Furthermore, TOR RNAi depletion in combination with *FASN1*$^{FB\text{-}RNAi}$ also mildly reduced FB glycogen similar to *InR*$^{FB\text{-}RNAi}$ reduction (**Fig 6C,D**).

Both insulin and TOR signaling control transcription factors important for metabolic rewiring during changes in animal feeding[38,77]. For example, a major downstream transcription factor along this axis is the sterol regulatory element-binding protein (SREBP), which facilitates lipid and fatty acid biosynthesis in mammals and *Drosophila*[43,78]. Therefore, we examined how RNAi depletion of *Drosophila* SREBP (*SREBP*$^{FB\text{-}RNAi}$*)* influenced glycogen storage when DNL was inhibited. Strikingly, dual depletion of SREBP and FASN1 led to a return of glycogen to near control levels (**Fig 6C,D**). In line with this, *SREBP* mRNA and protein levels were significantly boosted in *FASN1*$^{FB\text{-}RNAi}$ larvae, suggesting SREBP-dependent signaling was stimulated by DNL blockage (**Fig 6E**). Collectively, this suggests that the TG:glycogen metabolic switch requires SREBP-dependent signaling, and potentially may involve the sensing of fatty acids altered upon FASN1 depletion.

Glycogen storage in *FASN1*$^{FB\text{-}RNAi}$ FBs requires HAT enzymes nej and Tip60

Acetyl-CoA serves as a basic building block for FASN1-mediated fatty acid production, but acetyl-CoA pools also facilitate histone acetylation, thereby coupling cellular metabolism to gene regulation[79–81]. SREBP signaling is also closely linked to acetyl-CoA pools as mammalian SREBP-1 is itself acetylated[82]. Given this, we hypothesized that the SREBP-dependent metabolic switch in the *Drosophila* FB may be regulated by acetyl-CoA, especially since DNL blockage would be expected to influence cellular acetyl-CoA concentrations. Indeed, metabolomics revealed that FB acetyl-CoA levels were ~6-fold higher in *FASN1*$^{FB\text{-}RNAi}$ FBs compared to controls (**Fig 7A**).

To investigate whether acetyl-CoA pools influence glycogen storage in *Drosophila*, we considered that ATPCL and acetyl-CoA synthetase (AcCoAS) are the two primary contributors to the cytoplasmic and nucleoplasmic acetyl-CoA pools in the FB, respectively[81,83,84]. Given this, we RNAi depleted ATPCL and AcCoAS alone or in combination with FASN1, and evaluated how this impacted FB glycogen. Notably, *ATPCL*$^{FB\text{-}RNAi}$ alone did not alter FB glycogen levels relative to controls, and its depletion in combination with FASN1 KD resulted in a slight glycogen reduction compared to *FASN1*$^{FB\text{-}RNAi}$. This suggested ATPCL only mildly influenced FB glycogen, and was not a major driver in the TG:glycogen metabolic switch (**Fig 7B,C**). In contrast, AcCoAS RNAi in combination with FASN1 KD led to more dramatic reduction of glycogen storage, which now appeared similar to controls (**Fig 7D,E**). This indicated that AcCoAS substantially influenced the TG:glycogen metabolic switch. Given that AcCoAS is known to influence nucleoplasmic acetyl-CoA[81,83,84], this opened the possibility that acetyl-CoA could potentially influence histone acetylation and metabolic rewiring during DNL inhibition.

To investigate this possibility, we examined molecular players regulating histone acetylation. Of note, mammalian SREBP-1 activity depends on the transcriptional co-activator CBP/p300 (nej in *Drosophila*), which possesses histone acetyltransferase (HAT) activity and promotes SREBP-1 transcription of target genes[82,85]. HATs catalyze the transfer of an acetyl group from acetyl-CoA to lysine on both transcription factors (such as SREBP) and histones, thereby promoting a relaxed chromatin structure facilitating transcription factor binding and gene expression[82,85,86]. To determine whether specific HATs contribute to the TG:glycogen metabolic switch in *FASN1*$^{FB\text{-}RNAi}$ FBs, we conducted a candidate-based RNAi screen of six major *Drosophila* HAT proteins representing the three major HAT families in *Drosophila*[87]: Mof, Chm, GCN5, Elp3, Tip60, and nej. Among these, HAT screening revealed that RNAi depletion of nej and Tip60

suppressed the boosted glycogen stores in *FASN1*$^{FB\text{-}RNAi}$ larvae, with nej depletion having a partial effect, and Tip60 an almost complete return to baseline glycogen (**Fig 7F,G**).

Based on these findings we propose a model where Tip60 and nej play a role in SREBP-dependent metabolic remodeling in the FB when DNL is blocked. This non-canonical SREBP-dependent metabolic switch boosts glycogen storage in response to fatty acid depletion, ensuring organismal survival at the cost of female reproductive fecundity (**Fig 8**).

Discussion:

Here we provide evidence for a cell autonomous TG:glycogen metabolic switch in *Drosophila* triggered by a genetic blockage of DNL, which dramatically elevates glycogen storage and glycolysis in the FB, thereby ensuring organismal survival and development in the absence of abundant fat stores. Using genetics and biochemical assays, we show this switch requires *Drosophila* SREBP, a lipid sensing and nutrient regulating transcription factor that normally promotes lipogenesis. A critical regulatory feature of *Drosophila* SREBP is that it senses intracellular fatty acids including palmitate and related membrane lipids[78,88]. Critically, in *Drosophila* palmitate inhibits SREBP proteolytic processing and activation, suggesting SREBP may be activated in response to the drop in fatty acids upon DNL blockage to promote metabolic rewiring and survival. Interestingly, palmitate is the major fatty acid produced by FASN1. Therefore, we hypothesize that DNL inhibition lowers FB intracellular palmitate levels, promoting SREBP activation and nuclear localization where it drives transcription of genes supporting glycogen storage and glycolysis. In support of this, culturing *FASN1*$^{FB\text{-}RNAi}$ larvae on a palmitate-rich diet suppressed glycogen accumulation, likely through SREBP inhibition. We propose this SREBP-mediated transcription is supported by nej and Tip60, HAT enzymes whose mammalian orthologs are known to enhance SREBP activity[82].

Mammals possess three SREBP isoforms—SREBP-1a, SREBP-1c, and SREBP-2. SREBP-1a and SREBP-1c support fatty acid and TG synthesis through insulin-dependent lipogenesis, whereas SREBP-2 primarily regulates membrane sterol homeostasis[42,43,77]. In contrast, *Drosophila* encode a single SREBP homolog that recapitulates many functions of the mammalian proteins. Under lipid-deficient conditions, SREBP transcriptionally activates lipogenic genes of the DNL pathway, notably ACC and FASN1, which generate palmitate and provide feedback regulation of SREBP activity[41,78,88]. The canonical function of SREBP does not typically support a role in carbohydrate or glycogen metabolism. However, a recent murine study revealed that silencing SREBP-1 in the mouse liver reduced glycogen deposits and blunted the expression and activity of glycogenic factors, suggesting a potentially conserved role for SREBP in glycogen regulation[74].

Activation of *Drosophila* SREBP by the PI3K/Akt/TOR pathway is required for lipogenesis during insulin-stimulated cell and organ growth[43]. Insulin and TOR signaling supports basal glycogen storage during feeding and developmental growth by promoting glucose uptake and activating glycogen synthase via inhibition of GSK3, but these effects are not known to depend on SREBP[37,73,73]. These reports are consistent with our findings that single RNAi knockdowns of *InR* and *TOR*, but not *SREBP* depletion, reduce FB glycogen levels (**Fig 6C,D**). We found blunting insulin and TOR signaling in FASN1-deficient fat body moderately reduced glucose accumulation. However, combined loss of SREBP in the *FASN1*$^{FB\text{-}RNAi}$ background resulted in a more pronounced reduction in glycogen. Although, SREBP is not canonically a glycogen regulating transcription factor downstream of this pathway, insulin/TOR signaling may still contribute to the TG:glycogen balance in this context. We propose that in the FB, *Drosophila* SREBP's lipid-sensing capabilities may play a more important role in regulating glycogen metabolism than its activation by insulin or TOR.

We find the glycogen boost observed in *FASN1*$^{FB\text{-}RNAi}$ larvae partially required nej, a transcriptional SREBP coactivator and histone acetyltransferase (HAT). Notably, its mammalian homologs CBP/p300 are known to promote SREBP-1 activity, and to enhance expression of its target genes through acetylation[87,89,90]. Furthermore, loss of Tip60, another HAT, completely suppressed the elevated glycogen stores in *FASN1*$^{FB\text{-}RNAi}$ larvae. In previous *Drosophila* studies, nej and Tip60 have been linked to essential processes including chromatin regulation, development, learning, stress response, and lifespan[86,90,91]. Moreover in mammals, Tip60 and CBP/p300 (nej) acetylate each other, reinforcing each other's activities[92]. Both nej and Tip60 transfer acetyl groups sourced from acetyl-CoA to lysines on target histone and non-histone proteins[85,87]. Acetyl-CoA pools were significantly increased in *FASN1*$^{FB\text{-}RNAi}$ FBs, and interestingly reduced acetyl-CoA channeling of into fatty acid synthesis has been shown to shift acetyl-CoA utilization to histone acetylation, facilitating transcriptional reprogramming[87,93]. Typically in mammals, acetyl-CoA for histone acetylation is generated by ATPCL, and a smaller proportion from free acetate and coenzyme A catalyzed by acetyl-CoA synthetase[79–81]. Despite this, we found that ATPCL knockdown in the *FASN1*$^{FB\text{-}RNAi}$ background only had a minor impact on FB glycogen pools. In contrast, AcCoAS-depletion reduced glycogen storage in *FASN1*$^{FB\text{-}RNAi}$ FBs to near control levels, suggesting AcCoAS activity and potentially its role in histone acetylation facilitates the TG:glycogen metabolic switch in *FASN1*$^{FB\text{-}RNAi}$ FB. In line with this, recent studies suggest that when cellular resources are limited, AcCoAS translocates to the nucleus and is recruited to chromatin where it promotes histone acetylation[83]. In contrast, *Drosophila* ATPCL was found to be dispensable for global histone acetylation and gene transcription[94], consistent with our observation that ATPCL depletion did not substantially impact glycogen levels in DNL inhibited FBs.

Drosophila must reach critical weight to achieve pupation and metamorphosis, and the biomass for this is proposed to typically come from FB lipids[20–22]. Our findings challenge this notion as we

find *FASN1*$^{FB\text{-}RNAi}$ larvae lack fat stores yet grow to full size and pupate without developmental delay. We hypothesize that the ~20-fold concentrated glycogen deposits in *FASN1*$^{FB\text{-}RNAi}$ FBs are sufficient to fuel development. Indeed, glycogen may help compensate for the biomass loss associated with fat loss due to glycogen's ability to absorb 3-5 times its weight in water, which may assist *FASN1*$^{FB\text{-}RNAi}$ larvae to reach critical weight[95]. Additionally, our data indicate that glycogen reserves, previously deemed dispensable for metamorphosis[6,8], are essential for *FASN1*$^{FB\text{-}RNAi}$ animals during pupal to pharate adult transition. In control animals, larval FB glycogen remains mostly intact during metamorphosis, as TG serves as the primary energy source. In contrast, in *FASN1*$^{FB\text{-}RNAi}$ animals FB glycogen is heavily metabolized to fuel metamorphosis, resulting in its depletion in pharate adults. This metabolic rewiring reveals a previously unappreciated versatility to *Drosophila* development.

Fat-depleted *Drosophila* maintain developmental integrity by rebalancing fat:carbohydrate metabolism, but does this expose new vulnerabilities to survival? *FASN1*$^{FB\text{-}RNAi}$ male and female flies were starvation sensitive, and both males and females displayed shorter median lifespans. Adults did not have detectable whole-body TG and even glycogen amounts were 50% lower than control flies. Indeed, the adult FB, which forms *de novo* a few days after eclosion[96,97], could not be found or isolated, suggesting that the adult FB in *FASN1*$^{FB\text{-}RNAi}$ flies may be absent or severely reduced. The glycogen measured in these animals likely originates from muscle, the other major glycogen storage tissue in adults[5,57]. Critically, fertility was also drastically reduced in *FASN1*$^{FB\text{-}RNAi}$ females, likely due to defective lipid delivery to the ovary need for its development[51–53]. Infertility is a common biological tradeoff when nutrients are scarce; for example animals may support development of certain organs at the cost of others during periods of scarcity[49]. TG-rich LDs of nurse cells are synthesized from DAG, 80% of which is exogenously resourced from free-floating cells of the dissociated larval FB that persist in the newly hatched fly[24,53]. We reason that lipophorin-mediated DAG delivery from *FASN1*$^{FB\text{-}RNAi}$ lipid-

deficient fat cells to the ovaries is limited, impacting reproduction. In line with this, subsequent apoptosis of egg chambers due to low lipid content is reported in other studies[98,99].

In closing, the existence of a TG:glycogen metabolic switch in the *Drosophila* FB suggests versatile adaptive capacity for the *Drosophila* bioenergetics developmental program. Similar TG:glycogen rewiring is anecdotally also observed in mammals. In mice when TG storage was genetically blocked in adipose by DGAT1 and DGAT2 ablation, mice exhibit modest but significant increases in glycogen storage[100]. Furthermore, human organs exhibit specific ratios of fat and glycogen nutrient reserves, but how these are balanced and adapt to changes in nutrient availability remain incompletely understood. Here, we provide evidence for unique metabolic rewiring in the fruit fly which may apply to diverse human tissues. It suggests remarkable plasticity to nutrient storage and utilization in the struggle to adapt and survive.

Acknowledgements:

We thank members of the Henne and DeBerardinis labs for helpful advice and discussions during the development of this study. We also thank Anastasiia Kovalenko for initial help profiling fat body LD phenotypes. This work is supported by grants from the Welch Foundation I-1873 (W.M.H), the National Institutes of Health (NIH) grants GM119768 (W.M.H), DK126887 (W.M.H.), the Ara Parseghian Medical Research Fund, and the UT Southwestern Endowed Scholars Program. T.P.M. and R.J.D. are supported by CPRIT grant RP180778. R.J.D. is supported by NIH grants R35CA220449 and P50CA196516. L.G.Z., T.P.M., and the CRI Metabolomics Facility are supported by the Cancer Prevention Research Institute of Texas (CPRIT Core Facilities Support Award RP240494).

Data and Information Availability:

All data related to this study is available in the materials and also available upon request.

MATERIALS AND METHODS

Fly cultures and strains

All *Drosophila* animal research was performed in accordance with NIH recommended policies. *Drosophila* L3 late feeding/pre-wandering larvae (~100-108 h After Egg Laying or AEL) were used for fat tissue microscopy and biochemical assays, unless otherwise stated. For lifespan and starvation assays, adult male and female flies were used. Flies were reared and maintained on standard fly food containing cornmeal, yeast, molasses (~5-10% sugars), and agar. The *Dcg-Gal4* fat body (FB)-specific driver[45] was provided by Jonathan M. Graff (former UTSW). *UAS-FASN1*^{RNAi} and all other *TRiP RNAi* lines, *UAS-mito-PyronicSF*, protein/organelle marker strains and other transgenic stocks used in this study were obtained from the Bloomington Stock Center (Bloomington, IN). Typically, 5 to 7 *Gal4* driver males were crossed with ~20-30 females from test *UAS* or control lines. All experimental crosses and controls were cultured at ~100-150 animals per vial (mid-density, which maintains metabolic stability, PMID: 25994086), in a fly incubator with a 12-hour light/dark cycle and maintained at 25°C for uniform transgene expression. Please see Table S1 for a list of *Drosophila* lines used.

Larval fat body staining

Late feeding L3 larvae were gently removed from inside the food media using a paintbrush and rinsed in water to remove food particles. Larval fat bodies (FBs) or guts were dissected in PBS using Dumont #5 forceps (Electron Microscopy Sciences). All tissues were fixed in 4% paraformaldehyde (PFA) for 20 min at room temperature and rinsed briefly in PBS prior to staining. Lipid droplets in FBs were stained by incubating FBs in 100 µM monodansylpentane (MDH) LD stain (Abgent) for 20 min at room temperature, in the dark. Next, FBs were rinsed in PBS and mounted on slides in SlowFade Gold antifade reagent with nuclear DAPI (Invitrogen) for subsequent imaging.

Female ovary dissection and staining

Ovaries from 7 to 10-day old adult females were dissected in PBS, fixed in 4% PFA for 20 min at room temperature. Following a brief wash in PBS, ovaries were incubated in CellMask Actin stain (1:1000) or Phalloidin (1:400 in PBS-T) for staining of F-actin structures, according to manufacturer's instructions (Invitrogen). LDs in ovaries were stained with BODIPY 493/503 C12 (1:500) for 30 mins in the dark. Excess stain from ovaries was removed by washing in PBS, then mounted in SlowFade Gold antifade reagent containing DAPI (Invitrogen) for imaging. Egg chambers within ovarioles of the ovaries were staged according to established morphological criteria described in literature[101–103].

Confocal fluorescence microscopy

Prepared slides were imaged using Zeiss LSM880 inverted laser scanning confocal microscope. Tissues stained with organelle dyes (LD: MDH/ BODIPY C12/Nile Red; F-actin: phalloidin) and those expressing transgenic fluorescent-tagged proteins (e.g., UAS-GFP; ER marker *UAS-Sec61B-TdT*; PM marker *UAS-mcd8-GFP*; pyruvate sensor *PyronicSF-GFP;* mitochondrial marker *UAS-MitoTimer*) were imaged using the appropriate channel filter DAPI/GFP/RFP. Most FBs were imaged using a 40X oil immersion objective, and adult female ovaries with 10X or 20X objective.

Light and other fluorescence microscopy

Whole 3L larvae without or with GFP-expressing (*Dcg-Gal4>UAS-GFP*) FBs were imaged using the Leica S8AP0 stereoscope and EVOS FL Cell Imaging System (ThermoFisher), respectively. Adult male and female flies were also imaged on Leica S8AP0 stereoscope.

Transmission electron microscopy

FB tissue was removed from *Drosophila* larvae, fixed in 2.5% (v/v) glutaraldehyde in 0.1 M sodium cacodylate buffer paraformaldehyde, and processed in the UT Southwestern Electron Microscopy Core Facility. They were post-fixed in 1% osmium tetroxide and 0.8% K3[Fe(CN6)] in 0.1 M sodium cacodylate buffer for 1 hour at room temperature. Cells were rinsed with water and en bloc stained with 2% aqueous uranyl acetate overnight. Next, they were rinsed in buffer and dehydrated with increasing concentration of ethanol, infiltrated with Embed-812 resin and polymerized in a 60°C oven overnight. Blocks were sectioned with a diamond knife (Diatome) on a Leica Ultracut UCT (7) ultramicrotome (Leica Microsystems) and collected onto copper grids, post stained with 2% aqueous uranyl acetate and lead citrate. Images were acquired on a JOEL 1400 Plus transmission electron microscope using a voltage of 120 kV.

Quantitative PCR

Whole RNA was extracted from FB tissues (25-30 larvae per biological replicate , n = 3) using Trizol reagent (Ambion Life Technologies) according to manufacturer's instructions. RNA was quantified by Denovix spectrophotometer, and 1 µg of RNA was reverse transcribed to cDNA using iScript cDNA Synthesis Kit (BioRad). QPCR was performed with cDNA using the SsoAdvanced Universal SYBR Green Supermix (BioRad) on the BioRad CFX96 Real-Time System; mRNA expression data were normalized to that of the fly housekeeping gene rp49. Primer sequences for all transcripts amplified are available upon request.

Glucose and Trehalose assays

Feeding larvae washed out from culture vials were collected in 630 µm mesh-fitted baskets (Genesee) and rinsed to get rid of adherent food particles. Larvae were dried and divided onto into piles (10–12 larvae each, n = 3) on a strip of parafilm. Larvae were bled by tearing the cuticle with Dumont 5 forceps (Electron Microscopy Sciences). Two µl of colorless hemolymph was aspirated from each pile and separately transferred to 96-well plates (Thermo-Scientific)

containing 0.1% N-Phenylthiourea (Sigma-Aldrich) in 50 µl PBS. 150 µl of Autokit Glucose reagent (Wako) was added to each well and incubated at room temperature for 20 min before measuring absorbance at 505 nm. Glucose concentration was calculated from a standard curve generated with manufacturer's glucose standards. For trehalose assays, 8 µl of dilute hemolymph was treated with 5 µl of (diluted 8X) porcine kidney trehalase (Sigma) overnight at 37 °C. Ten µl of treated sample was assayed for trehalose as described for glucose. Trehalose amounts were calculated from standard glucose, as for glucose.

Glycogen assay

Whole animals (10 larvae/pharate pupae/adults per biological replicate, n = 3) or dissected FBs (25-30 larvae per biological replicate, n = 3) were homogenized in 300 µl ice-cold PBS using a pestle or sonication and syringe (29G1/2 needle), respectively. After reserving 20 µl of the homogenate for protein Bradford quantification, the rest of the homogenate was heat inactivated at 70°C for 10 min. Homogenate was then centrifuged at maximum speed at 4°C for 10 min and supernatant was collected in a new tube. In a 96-well plate, 30 µl of each sample was loaded in duplicate rows. Then, 100 µl of Autokit Glucose reagent + amyloglucosidase (2 µl amyloglucosidase {Sigma A1602; 25mg} per 1 ml of Glucose reagent) was added to one row of samples, and 100 µl of Glucose reagent alone (without amyloglucosidase) was added to the duplicate row of samples, and to the glucose standards. The plate was incubated at 37°C for 30 min, after which color intensity was measured using a microplate reader at 505 nm. Free glucose concentration in treated and untreated samples was calculated based on the glucose standard curve. Glycogen concentration (as free glucose) was determined by subtracting glucose in the untreated samples from those treated with amyloglucosidase. Finally, total glycogen was normalized to protein measured by the Bradford assay.

Periodic Acid-Schiff stain

Glycogen in FB tissues from late feeding L3 larvae was stained using the Periodic Acid-Schiff (PAS) kit (Sigma). Larval FBs were dissected in 1% BSA in PBS, fixed with 4% paraformaldehyde for 20 min, and washed twice with 1% BSA in PBS. FBs were then incubated in 0.5% period acid solution for 5 min, washed twice with 1% BSA in PBS, then stained with Schiff's reagent for 15 min, washed again, and mounted on slides. PAS-stained FB tissues were imaged using the Leica DM6B light microscope. Comparative PAS staining intensity was quantified using Fiji ImageJ software, with an average of ~12 independent FBs analyzed per sample, except for *Dcg* control and *FASN1*$^{FB\text{-}RNAi}$ (n ≥ 25 each).

Thin layer chromatography

Late feeding L3 larvae or adult flies (10 per biological replicate, n = 3) were weighed, then homogenized in 2:1:0.8 of methanol:chloroform:water. Please see **Table S4** and **Table S5** for more details on these measurements. Samples were incubated in a 37°C water bath for 1 hour. Chloroform and 1M KCl (1:1) were added to the sample, centrifuged at 3000 rpm for 2 min, and the bottom layer containing lipids was aspirated using a syringe. Lipids were dried using argon gas and resuspended in chloroform (100 µl of chloroform/7mg of fly weight). Extracted lipids alongside serially diluted standard neutral lipids of known concentrations were separated on TLC plates using hexane:diethyl ether:acetic acid solvent (80:20:1, v/v/v). TLC plate was air dried for 10 min, spray stained with 3% copper (II) acetate in 8% phosphoric acid and incubated at 145°C in the oven for 30 min to 1 hour to allow bands to develop for scanning and imaging. Neutral lipid (TAG) band intensity was quantified using Fiji ImageJ software, and lipid concentrations were calculated from the standard curve generated with standard mixture. In the case of dissected larval guts (20-30 mid-guts, n = 3) dried lipids for all samples were re-suspended in 120 µl of chloroform and final lipid concentrations were calculated by normalizing to protein in sample, measured by standard Bradford assay.

Adult starvation assay

Freshly emerging adult flies were collected over a period of 1 to 3 days and transferred to fresh standard food bottles. Flies were aged for 7 to 10 days, then male and female flies were separately moved to food-free vials (10 flies per biological replicate, n = 3) containing a cotton plug at the bottom soaked with 2 ml of tap water. Flies were kept at 25°C and vials were examined at least 3X daily to record number of dead flies. Surviving flies were moved to fresh vials with water-soaked plug every 24 hours for optimal hydration and to avoid fungal growth.

Adult lifespan assay

Flies hatching between 0 to 3 hours were pooled, and 100 males and 100 females were separately placed in fresh standard food vials (20 flies per vial). Vials were maintained at 25°C, and dead flies were scored daily while moving surviving flies to fresh food.

Adult survivorship assay

Double FB-KDs of FASN1 and candidate genes were generated by crossing 5 to 7 *Dcg-Gal4>UAS-FASN1-RNAi* males to ~20 females from candidate *UAS-RNAi* line in standard food vials cultured at 25°C. Mated females were allowed to lay eggs for 2 days, then parents were removed to fresh vials. Larvae carrying *Dcg-Gal4* driver + both *UAS-RNAi* transgenes were identified and moved to a new vial for developmental monitoring. Animals successfully completing metamorphosis and hatching into adult flies were scored. This count was compared to adult survivorship of *Dcg-Gal4 control*, *Dcg-Gal4>UAS-FASN1-RNAi*, *Dcg-Gal4>cand UAS-RNAi* animals.

Fertility assays

All parents (*Dcg-Gal4* and *UAS-FASN1-RNAi* males and females) used were 7 to 10 days old. 10 virgin females were crossed with 10 males in fresh food vials streaked with yeast paste and

kept overnight at 25°C. The following morning, flies were flipped to new food at 1 hour intervals (3X) to empty females of older eggs/embryos. Flies were then allowed to lay on fresh plates supplemented with a drop of yeast paste for 4-6 hours, following which all parents were removed from bottles and number of eggs laid was counted. The hatching of eggs on the food surface and development of progeny was closely monitored and recorded.

Sample preparation for proteomic profiling

Fat bodies were extracted from late feeding L3 larvae (60-80 larvae per biological replicate, n = 3) in chilled Lysis Buffer + protease inhibitor cocktail. Tissues were homogenized by sonication and supernatant (lysate) was collected after centrifugation for 30 sec at 1000xg at 4°C. Centrifugation was repeated at 16,000xg for 10 min at 4°C, and supernatant transferred to fresh Eppendorf tube. Sample for loading was prepared by mixing protein sample with 2X LDS Sample Buffer and Lysis Buffer, and boiling at 95°C for 5 min. Sample was run on a 10% pre-cast polyacrylamide gel (BioRad) at 100 V for ~25 min until the dye front was past the ladder. Gel was rinsed in MQ-water, then stained with Coomassie BB R250 in 10% acetic acid, 50% methanol, 40% water for 20 min at room temperature with rocking. Subsequently, gel was de-stained for 1 hour in 10% acetic acid, 50% methanol, 40% water with 4 solvent changes. When gel background appeared clear, de-stain was exchanged for water. Protein gel bands were cut on clean glass surface of gel imager with new razor, diced into 1 mm cubes, and moved to sterile Eppendorf tubes on ice for delivery to Proteomics Core Facility at UTSW for protein identification by mass spectrometry.

Sample preparation for metabolomic profiling

Fat tissues dissected from late feeding L3 larvae (60-80 larvae per biological replicate, n = 3) were homogenized in ice-cold methanol/water 80:20 (vol/vol) using a sonicator. Lysate was subjected to three freeze-thaw cycles between liquid nitrogen and 37 °C, vortexed vigorously,

and then centrifuged at ~20,160xg for 15 min at 4°C. Protein in the supernatant was measured using the Pierce BCA kit, and volume containing 10 µg protein was dried in a SpeedVac. Sample was re-suspended in 100 uL acetonitrile/water 80:20 (vol/vol), vortexed for 1 min, and centrifuged at ~20,160xg for 15 min at 4°C. Metabolite-containing supernatant was transferred to a fresh Eppendorf tube and submitted to the CRI Metabolomics Facility at UTSW for LC-MS metabolite analyses. Metabolites were quantified as described previously [104,105].

Statistical analysis

Experimental findings were validated through independent biological replicates, with assays repeated at least three times. For the figures, all comparative statistics were assessed by two-tailed Student's T-test. Statistical significance was applied if $p<0.05$. Error bars indicate SD. In general, a single * indicates $p<0.05$, ** indicates $p<0.01$, *** indicates $p<0.001$, **** indicates $p<0.0001$.

Figure Legends:

Figure 1: Loss of FASN1 in *Drosophila* fat body produces virtually fat less flies

A) Cartoon of RNA interference-mediated KD using the UAS/Gal4 system; parental cross between females carrying tissue (fat body)-specific *Dcg-Gal4* driver and males containing the *UAS-FASN1*^{RNAi} transgene generate progeny lacking *FASN1* in the FB.
B) (Top panel) *Dcg-Gal4* control and *FASN1*$^{FB\text{-}RNAi}$ (*Dcg-Gal4>UAS-FASN1*^{RNAi}) age-matched late feeding/pre-wandering third instar (L3) larvae. *Dcg-Gal4/Dcg-Gal4* and *Dcg-Gal4>mCherry*^{RNAi} were used as controls. Scale bar 1 mm. (Bottom panel). Fluorescence micrograph of *Dcg-Gal4* control and *FASN1*$^{FB\text{-}RNAi}$ larvae expressing soluble GFP in their FBs (*Dcg-Gal4>UAS-GFP*). Scale bar 2mm.
C) Confocal images of *Dcg-Gal4* control and *FASN1*$^{FB\text{-}RNAi}$ FBs from L3 pre-wandering larvae expressing a membrane-associated reporter (*Dcg-Gal4>UAS-Glut4-GFP*) to visualize cell boundaries.

D) FB cell sizes for *Dcg-Gal4* control and *FASN1*$^{FB\text{-}RNAi}$ FBs from L3 larvae. (n ≥ 249 FB cells each)

E) Confocal images of *Dcg-Gal4* control and *FASN1*$^{FB\text{-}RNAi}$ larval (L3) FB periphery and mid-plane sections stained with LD stain monodansylpentane (MDH). Scale bar 50 µm.

F) Confocal images of Dcg-Gal4 control and *FASN1*$^{FB\text{-}RNAi}$ FBs at their mid-plane and periphery from larvae expressing ER marker (*Dcg-Gal4>UAS-Sec61B-tDTomato*) and stained with MDH. *FASN1* loss results in adipocytes empty of LDs. Scale bar 10 µm.

G) TEM micrographs of *Dcg-Gal4* control and *FASN1*$^{FB\text{-}RNAi}$ FB cells showing peripheral LDs (pLDs, red arrows). *FASN1*$^{FB\text{-}RNAi}$ cell appears vacant of medial LDs (mLDs) and contains little 'islands' of ER, LDs, and other organelles (green arrows). Scale bar 2-4 µm.

H) Total triglycerides (TG) measured by thin layer chromatography (TLC) in whole L3 pre-wandering *Dcg-Gal4* control and *FASN1*$^{FB\text{-}RNAi}$ larvae. TLC plate showing TG bands corresponding to the quantified samples is shown below the graph. (10 larvae per biological replicate, n = 3).

I) Pupal sizes (Length = L, Width = W) for *Dcg-Gal4* control and *FASN1*$^{FB\text{-}RNAi}$ pupae. (n = 27 each) measured using digital Vernier calipers.

Statistical significance was assessed using a two-tailed Student's t-test ($P < 0.05$); error bars denote standard deviation (SD).

Figure 2: *FASN1*-deficient flies are viable but exhibit increased starvation sensitivity, reduced lifespan, and female fertility defects

A) Size comparison of *Dcg-Gal4* control and *FASN1*$^{FB\text{-}RNAi}$ female (left) and male (right) adult flies. Scale bar 2 mm.

B) Weights of female and male *Dcg-Gal4* control and *FASN1*$^{FB\text{-}RNAi}$ adult flies (aged 7-10 days). Males and female flies were weighed separately in groups of 10 (n = 9).

C) Total triglycerides (TG) measured by thin layer chromatography (TLC) in *Dcg-Gal4* control and *FASN1*$^{FB\text{-}RNAi}$ female and male flies. TLC plate showing TG bands corresponding to the quantified samples is shown below the graph. (10 flies per biological replicate, n = 3).

D) Longevity assay performed for control (*Dcg-Gal4*) and *FASN1*$^{FB\text{-}RNAi}$ adult females and males (20 flies per vial, n = 5).

E) Starvation assay using 7-10 days old control and *FASN1*$^{FB\text{-}RNAi}$ female and male flies (10 flies per vials, n = 3).

F) Fertility assay performed to test viability of eggs produced by control (*Dcg-Gal4*) or *FASN1*$^{FB\text{-}RNAi}$ females mated with either *Dcg-Gal4* or *FASN1*$^{FB\text{-}RNAi}$ males.

G) Confocal images of ovaries from 7–10-day old *Dcg-Gal4* control and *FASN1*$^{FB\text{-}RNAi}$ adult females stained with CellMask Actin stain. Entire *FASN1*$^{FB\text{-}RNAi}$ ovary (right) is visible at 10X magnification. Parts of the control ovary are labelled (left). Scale bar 200 µm.

H) Confocal images of ovaries from *Dcg-Gal4* control and *FASN1*$^{FB\text{-}RNAi}$ females stained with CellMask Actin stain. Yellow arrows point to follicle cells of stage 9/10 egg chambers. White arrows point to oocyte; oocyte maturation fails in *FASN1*$^{FB\text{-}RNAi}$ ovaries. Scale bar 100 µm.

I) Confocal images of LDs in control and *FASN1*$^{FB\text{-}RNAi}$ ovaries stained with BODIPY. Orange arrow in control ovary indicates LDs accumulated in nurse cells and purple arrow shows ring canal where movement of LDs from nurse cells to the developing oocyte is occurring. There also appear to be plentiful LDs in the mature oocyte*. LDs are sparse in *FASN1*$^{FB\text{-}RNAi}$ egg chambers. Scale bar 200 µm.

Statistical significance was assessed using a two-tailed Student's t-test ($P < 0.05$); error bars denote standard deviation (SD).

Figure 3: *FASN1*-deficient larvae channel dietary glucose to glycogen as energy reserves

A) Principal Component Analysis (PCA) for global proteomics performed in FBs isolated from *Dcg-Gal4* control and *FASN1*$^{FB\text{-}RNAi}$ L3 larvae.

B) Volcano plot of proteins detected by LC-MS/MS analyses performed in FBs isolated from *Dcg-Gal4* control and *FASN1*$^{FB\text{-}RNAi}$ L3 larvae.

C) Lipid metabolism processes were revealed to be amongst the most downregulated in *FASN1*$^{FB\text{-}RNAi}$ FBs. GO enrichment analysis of proteomics data was performed using Pangea.

D) Carbohydrates metabolism processes downregulated in *FASN1*$^{FB\text{-}RNAi}$ FBs (Pangea).

E) Relative expression of *tobi* mRNA in isolated FBs from *Dcg-Gal4* control and *FASN1*$^{FB\text{-}RNAi}$ larvae, measured by QPCR.

F) Periodic acid-Schiff (PAS) glycogen stain of larval FBs from *Dcg-Gal4* control and *FASN1*$^{FB\text{-}RNAi}$ larvae. Scale bar 50 µm.

G) Quantification of glycogen extracted from *Dcg-Gal4* control and *FASN1*$^{FB\text{-}RNAi}$ larval FBs.

H) Percentage of L3 larvae (*Dcg-Gal4* control, *FASN1*$^{FB\text{-}RNAi}$, *GlyS*$^{FB\text{-}RNAi}$, *FASN1*$^{FB\text{-}RNAi}$+ *GlyS*$^{FB\text{-}RNAi}$) successfully completing metamorphosis to yield adult flies. ($n \geq 60$ each).

I) Percentage of L3 larvae (*Dcg-Gal4* control, *FASN1*$^{FB\text{-}RNAi}$, *tobi*$^{FB\text{-}RNAi}$, *FASN1*$^{FB\text{-}RNA\ i}$+ *tobi*$^{FB\text{-}RNAi}$) successfully completing metamorphosis to adult flies. (n ≥ 60 each). Statistical significance was assessed using a two-tailed Student's t-test (P < 0.05); error bars denote standard deviation (SD).

Figure 4: Larvae lacking FASN1 elevate glycolysis while down-regulating mitochondrial TCA and ETC

A) Schematic representing the fate of glucose and role of FASN1 in *de novo* lipogenesis.
B) Relative increases (delta fold) in protein levels of glycolysis enzymes in *FASN1*$^{FB\text{-}RNAi}$ FBs revealed by proteomics profiling.
C) Expression of fluorescent pyruvate biosensor *UAS-PyronicSF-GFP* in control and *FASN1*$^{FB\text{-}RNAi}$ larval FBs: Fire-LUT pseudo-colored (Fiji). Scale Bar 50 µm.
D) Percentage of L3 larvae (control, *FASN1*$^{FB\text{-}RNAi}$, *Pyk*$^{FB\text{-}RNAi}$, *FASN1*$^{FB\text{-}RNAi}$+ *Pyk*$^{FB\text{-}RNAi}$) successfully completing metamorphosis to adult flies. (n ≥ 40 each).
E) Percentage of L3 larvae (control, *FASN1*$^{FB\text{-}RNAi}$, *Ldh*$^{FB\text{-}RNAi}$, *FASN1*$^{FB\text{-}RNA\ i}$+ *Ldh*$^{FB\text{-}RNAi}$) completing development to adult flies. (n ≥ 30 each).
F) Relative changes (delta fold) in tricarboxylic acid cycle (TCA) enzymes in *FASN1*$^{FB\text{-}RNAi}$ FBs detected by global proteomics.
G) Relative expression of *ATPCL* in FBs from *Dcg-Gal4* control and *FASN1*$^{FB\text{-}RNAi}$ larvae, measured by QPCR.
H) Confocal images of *Dcg-Gal4* control and *FASN1*$^{FB\text{-}RNAi}$ FBs stained with MitoSOX Green. Scale Bar 20 µm.
I) Quantification of MitoSOX Green signal intensity in *Dcg-Gal4* control and *FASN1*$^{FB\text{-}RNAi}$ FBs.
J) Heat map of LC-MS/MS metabolomics showing raw abundances (colored by row) of upregulated and downregulated TCA and FAO metabolites in the FBs of *FASN1*$^{FB\text{-}RNAi}$ larvae relative to *Dcg-Gal4* controls.

Statistical significance was assessed using a two-tailed Student's t-test (P < 0.05); error bars denote standard deviation (SD).

Figure 5: Disruption of fatty acid synthesis during early *de novo* lipogenesis (DNL) drives a metabolic rewiring that favors glycogen storage over triglyceride accumulation.

A) Periodic Acid-Schiff (PAS) staining of glycogen in larval FBs with RNAi knockdown of key enzymes in DNL pathway. Scale bar 50 µm.

B) PAS glycogen stain in FB upon depletion of factors known to regulate lipid storage Scale bar 50 µm.

C) Quantification of PAS glycogen staining intensity (measured as inverted mean gray value)
in DNL-KD FBs (A).

D) Quantification of PAS glycogen staining intensity in FBs RNAi-targeted for lipid storage genes (B).

E) (*Top panel*) Confocal section images of FB periphery and mid-plane stained with LD stain MDH. FBs from the ubiquitous but mosaic driver *da-Gal4* (control) and *da-Gal4>UAS-FASN1*^{RNAi} L3 larvae also express PM marker mcd8-GFP; green indicates where *da-gal4* is expressed, and where *FASN1*-KD also occurs (right only). Scale bar 50 µm. **E'** (*Bottom panel*). PAS glycogen stain in FBs from driver *da-Gal4* and *da-Gal4>UAS-FASN1*^{RNAi}. White arrows indicate where *da-gal4* is expressed and *FASN1*-KD occurs (stronger PAS stain). Blue arrows point to regions where *FASN1* KD is inactive. Scale bar 50µm.

F) PAS glycogen staining in FBs from *Dcg-Gal4* control and *FASN1*$^{FB\text{-}RNAi}$ cultured in standard food and food supplemented with 10% Palm Oil (PO). Scale bar 50 µm.

G) Quantification of PAS glycogen staining intensity (inverted mean gray value) in FBs from *Dcg-Gal4* control and *FASN1*$^{FB\text{-}RNAi}$ cultured in standard food and 10% PO food. Statistical significance was assessed using a two-tailed Student's t-test ($P < 0.05$); error bars denote standard deviation (SD).

Figure 6: A candidate screen identifies SREBP as a critical determinant of the TG-to-glycogen storage shift.

A) PAS staining of glycogen in larval FBs upon *kdn* KD (*kdn*$^{FB\text{-}RNAi}$) or overexpression (*UAS-kdn*^{FB}) in the presence or absence of *FASN1*, stained with LD stain MDH. Scale Bar 50 µm.

B) Quantification of PAS glycogen staining intensity of (A), measured as inverted mean gray value.

C) PAS glycogen stain in FBs following single loss-of-function of InR, TOR, and SREBP, or in combination with FASN1 depletion. Scale Bar 50 µm.

D) Quantification of PAS glycogen staining intensity of (C), measured as inverted mean gray value.

E) Relative expression of SREBP mRNA (by QPCR) and protein (by LC-MS/MS proteomics) detected in FASN1-deficient FBs

Statistical significance was assessed using a two-tailed Student's t-test ($P < 0.05$); error bars denote standard deviation (SD).

Figure 7: *FASN1*$^{FB\text{-}RNAi}$ rewire metabolism through acetyl-CoA-dependent Nej and Tip60-HAT activity

A) Relative acetyl-CoA amounts in *FASN1*$^{FB\text{-}RNAi}$ FBs detected by metabolomic profiling.

B) Periodic Acid-Schiff (PAS) staining of glycogen in larval FBs following ATPCL inhibition alone (*ATPCL*$^{FB\text{-}RNAi}$), or together with FASN1-RNAi. Scale bar 50 µm.

C) Quantification of PAS glycogen staining intensity of (A), measured as inverted mean gray value.

D) PAS glycogen stain in FBs upon individual *AcCoAS* loss-of-function (*AcCoAS*$^{FB\text{-}RNAi}$), or in combination with FASN1-RNAi. Scale bar 50 µm.

E) Quantification of PAS glycogen staining intensity of (C), measured as inverted mean gray value.

F) PAS glycogen stain in FBs following KD of histone acetyltransferases (HATS), *Nej*$^{fB\text{-}RNAi}$ and *Tip60*$^{FB\text{-}RNAi}$ alone, or concomitant FASN1 loss. Scale Bar 50 µm.

G) Quantification of PAS glycogen staining intensity of (E), measured as inverted mean gray value.

Statistical significance was assessed using a two-tailed Student's t-test ($P < 0.05$); error bars denote standard deviation (SD).

Figure 8: Working model for how triglyceride:carbohydrate cross-talk and metabolic re-wiring occurs in a ‘fat-less’ *Drosophila* model to promote growth and development

Supplemental Figures:

SFigure 1:

A) Relative expression of *FASN1* mRNA in *Dcg-Gal4* control and *Dcg-Gal4>UAS-FASN1*^{RNAi} (*FASN1*$^{FB\text{-}RNAi}$) FBs.

B) Buoyancy-based test of fat content on extracted FBs from control and *FASN1*$^{FB\text{-}RNAi}$ larvae.

C) Confocal images of FB periphery and mid-plane sections from *Dcg-Gal4* control alongside FASN loss-of-functions isoforms (*FASN1*$^{FB\text{-}RNAi}$, *FASN2* global mutant, *FASN3*$^{FB\text{-}RNAi}$), stained with LD stain monodansylpentane (MDH). Scale bar 50 µm.

D) Relative triglycerides (TG) in isolated larval guts from control and *FASN1*$^{FB\text{-}RNAi}$ L3 larvae.

E) Confocal images of FB mid-plane sections from *Dcg-Gal4*, *Cg-Gal4*, and *r4-Gal4* driver control alongside their respective *FASN1* loss-of-function counterparts, stained with LD stain MDH. Scale bar 50 µm.

F) Control and *FASN1*$^{FB\text{-}RNAi}$ larval hemolymph glucose levels (mg/DL).

G) Control and *FASN1*$^{FB\text{-}RNAi}$ larval hemolymph trehalose levels (mg/DL).

Statistical significance was assessed using a two-tailed Student's t-test ($P < 0.05$); error bars denote standard deviation (SD).

SFigure 2:

A) Confocal images of phalloidin-stained ovaries from control and *FASN1*$^{FB\text{-}RNAi}$ females. White arrows point to mature oocyte in control ovary and arrested oocyte in *FASN1*$^{FB\text{-}RNAi}$. Scale bar (10X) 200 µm, Scale bar (20X) 100 µm.

B) Confocal images of LDs in control and *FASN1*$^{FB\text{-}RNAi}$ ovaries stained with BODIPY. Orange arrow in control ovary indicates LDs accumulated in nurse cells and purple arrow shows ring canal where movement of LDs from nurse cells to the developing oocyte is occurring. There also appear to be plentiful LDs in the mature oocyte*. LDs are sparse in *FASN1*$^{FB\text{-}RNAi}$ egg chambers.

SFigure 3:

A) Confocal images of control and *FASN1*$^{FB\text{-}RNAi}$ larval FB periphery and mid-plane sections expressing Glycogenin-YFP and stained with nuclear DAPI. Scale bar 50 µm.

B) QPCR expression profiles of genes related to glycogenesis and glycogenolysis in FBs from control (Dcg-Gal4) and Dcg-Gal4>FASN1 RNAi.

C) Relative change in Glo1 protein expression in *FASN1*$^{FB\text{-}RNAi}$ FBs, detected by global proteomics.

D) Relative TG and glycogen levels measured in *Dcg-Gal4* control and *FASN1*$^{FB\text{-}RNAi}$ animals during metamorphosis: Feeding Larvae FL (~100-108 h AEL), Pharate Adults PA (~205-215 AEL), AEL = After Egg Laying.

E) Relative changes (delta fold) in TG and glycogen in *Dcg-Gal4* control and *FASN1*$^{FB\text{-}RNAi}$ animals during metamorphosis.

F) Relative glycogen measured in *Dcg-Gal4* control and *FASN1*$^{FB\text{-}RNAi}$ male and female flies. (10 flies per biological replicate, n = 3).

Statistical significance was assessed using a two-tailed Student's t-test ($P < 0.05$); error bars denote standard deviation (SD).

SFigure 4:

A) Gene expression (delta fold) changes in pyruvate metabolism enzymes in *FASN1*$^{FB\text{-}RNAi}$ FBs relative to controls, measured by QPCR.

B) Relative changes (delta fold) in mRNA and protein levels of Idh in *FASN1*$^{FB\text{-}RNAi}$ FBs compared to controls.

C) Relative changes (delta fold) in electron transport chain (ETC) enzymes in *FASN1*$^{FB\text{-}RNAi}$ FBs detected by global proteomics.

D) Relative changes (delta fold) in mitochondrial fatty acid oxidation (FAO) enzymes in *FASN1*$^{FB\text{-}RNAi}$ FBs detected by global proteomics.

Statistical significance was assessed using a two-tailed Student's t-test ($P < 0.05$); error bars denote standard deviation (SD).

SFigure 5:

A) Confocal images of FBs from RNAi lines targeting DNL enzymes, stained with LD stain MDH. Scale Bar 25 µm.

B) Confocal images of FBs following RNA depletion of lipid storage genes, stained with the LD stain MDH. Scale Bar 25 µm.

C) Confocal images of MDH-stained LDs in FBs from *Dcg-Gal4* control and *FASN1*$^{FB\text{-}RNAi}$ cultured on standard food and 10% Palm Oil (PO). Scale Bar 50 µm.

SFigure 6:

A) PAS glycogen staining in FBs upon AMPK activation (*UAS-AMPK*^{FB}), or in combination with FASN1 depletion. Scale Bar 50 µm

B) Quantification of PAS glycogen staining intensity of (A), measured as inverted mean gray value.

C) Relative Citrate amounts in *FASN1*$^{FB\text{-}RNAi}$ FBs detected by metabolomic profiling.

D) Comparison of PAS glycogen stain in FB with single KDs of *Pfk* and *FASN1*, relative to *Dcg-Gal4* control.

E) Quantification of PAS glycogen staining intensity of (D), measured as inverted mean gray value.

Statistical significance was assessed using a two-tailed Student's t-test ($P < 0.05$); error bars denote standard deviation (SD).

Supplemental Tables:

Table S1: List of Drosophila stock lines used in this study.

Table S2: Mass spectrometry proteomics dataset for isolated larval fat bodies. The FASN1 larval fat body specific RNAi knockdown is compared to Dcg-Gal4 control fat bodies. The three FASN1 KD repeats are listed on sheet two as FASN 1-3. Dcg-Gal4 control fat bodies are Dcg 1-3.

Table S3: LC-MS metabolomics profiles for soluble metabolites from isolated Drosophila larval fat bodies. FASN1 fat body specific KD fat bodies (denoted RNAi KD) are compared to Dcg-Gal4 control (Ctrl) fat bodies.

Table S4: Sample weights for preparation of *Drosophila* larvae, with details on how samples were processed for lipid extraction and TLC processing.

Table S5: Sample weights for preparation of *Drosophila* flies, with details on how samples were processed for lipid extraction and TLC processing.

References:

1. Schönborn, J. W., Jehrke, L., Mettler-Altmann, T. & Beller, M. FlySilico: Flux balance modeling of Drosophila larval growth and resource allocation. *Sci. Rep.* **9**, 17156 (2019).
2. Wong, K. K. L., Liao, J. Z. & Verheyen, E. M. A positive feedback loop between Myc and aerobic glycolysis sustains tumor growth in a Drosophila tumor model. *eLife* **8**, e46315 (2019).
3. Chatterjee, N. & Perrimon, N. What fuels the fly: Energy metabolism in Drosophila and its application to the study of obesity and diabetes. *Sci. Adv.* **7**, eabg4336 (2021).
4. Garrido, D. *et al.* Fatty acid synthase cooperates with glyoxalase 1 to protect against sugar toxicity. *PLoS Genet.* **11**, e1004995 (2015).
5. Mattila, J. & Hietakangas, V. Regulation of Carbohydrate Energy Metabolism in Drosophila melanogaster. *Genetics* **207**, 1231–1253 (2017).
6. Gáliková, M. & Klepsatel, P. Endocrine control of glycogen and triacylglycerol breakdown in the fly model. *Semin. Cell Dev. Biol.* **138**, 104–116 (2023).
7. Meschi, E. & Delanoue, R. Adipokine and fat body in flies: Connecting organs. *Mol. Cell. Endocrinol.* **533**, 111339 (2021).
8. Gáliková, M. *et al.* Energy Homeostasis Control in Drosophila Adipokinetic Hormone Mutants. *Genetics* **201**, 665–683 (2015).
9. Miao, T. *et al.* Acetyl-CoA-mediated autoacetylation of fatty acid synthase as a metabolic switch of de novo lipogenesis in Drosophila. *Proc. Natl. Acad. Sci. U. S. A.* **119**, e2212220119 (2022).
10. Musselman, L. P. & Kühnlein, R. P. Drosophila as a model to study obesity and metabolic disease. *J. Exp. Biol.* **221**, jeb163881 (2018).
11. Walls, S. M. *et al.* Ceramide-Protein Interactions Modulate Ceramide-Associated Lipotoxic Cardiomyopathy. *Cell Rep.* **22**, 2702–2715 (2018).

12. Baker, K. D. & Thummel, C. S. Diabetic larvae and obese flies-emerging studies of metabolism in Drosophila. *Cell Metab.* **6**, 257–266 (2007).

13. Verheyen, E. M. The power of Drosophila in modeling human disease mechanisms. *Dis. Model. Mech.* **15**, dmm049549 (2022).

14. Musselman, L. P. *et al.* A high-sugar diet produces obesity and insulin resistance in wild-type Drosophila. *Dis. Model. Mech.* **4**, 842–849 (2011).

15. Ugrankar, R., Liu, Y., Provaznik, J., Schmitt, S. & Lehmann, M. Lipin is a central regulator of adipose tissue development and function in Drosophila melanogaster. *Mol. Cell. Biol.* **31**, 1646–1656 (2011).

16. Ugrankar, R. *et al.* Drosophila glucome screening identifies Ck1alpha as a regulator of mammalian glucose metabolism. *Nat. Commun.* **6**, 7102 (2015).

17. Arrese, E. L. & Soulages, J. L. Insect fat body: energy, metabolism, and regulation. *Annu. Rev. Entomol.* **55**, 207–225 (2010).

18. Musselman, L. P. *et al.* Role of fat body lipogenesis in protection against the effects of caloric overload in Drosophila. *J. Biol. Chem.* **288**, 8028–8042 (2013).

19. Chng, W.-B. A., Hietakangas, V. & Lemaitre, B. Physiological Adaptations to Sugar Intake: New Paradigms from Drosophila melanogaster. *Trends Endocrinol. Metab. TEM* **28**, 131–142 (2017).

20. Jacobs, H. T., George, J. & Kemppainen, E. Regulation of growth in Drosophila melanogaster: the roles of mitochondrial metabolism. *J. Biochem. (Tokyo)* **167**, 267–277 (2020).

21. Nishimura, T. Feedforward Regulation of Glucose Metabolism by Steroid Hormones Drives a Developmental Transition in Drosophila. *Curr. Biol. CB* **30**, 3624-3632.e5 (2020).

22. Tennessen, J. M. & Thummel, C. S. Coordinating growth and maturation - insights from Drosophila. *Curr. Biol. CB* **21**, R750-757 (2011).

23. Aguila, J. R., Suszko, J., Gibbs, A. G. & Hoshizaki, D. K. The role of larval fat cells in adult Drosophila melanogaster. *J. Exp. Biol.* **210**, 956–963 (2007).

24. Heier, C., Klishch, S., Stilbytska, O., Semaniuk, U. & Lushchak, O. The Drosophila model to interrogate triacylglycerol biology. *Biochim. Biophys. Acta Mol. Cell Biol. Lipids* **1866**, 158924 (2021).

25. Merkey, A. B., Wong, C. K., Hoshizaki, D. K. & Gibbs, A. G. Energetics of metamorphosis in Drosophila melanogaster. *J. Insect Physiol.* **57**, 1437–1445 (2011).

26. Ugrankar, R., Liu, Y., Provaznik, J., Schmitt, S. & Lehmann, M. Lipin is a central regulator of adipose tissue development and function in Drosophila melanogaster. *Mol. Cell. Biol.* **31**, 1646–1656 (2011).

27. Cartwright, B. R. *et al.* Seipin performs dissectible functions in promoting lipid droplet biogenesis and regulating droplet morphology. *Mol. Biol. Cell* **26**, 726–739 (2015).

28. Tian, Y. *et al.* Tissue-autonomous function of Drosophila seipin in preventing ectopic lipid droplet formation. *PLoS Genet.* **7**, e1001364 (2011).

29. Yamada, T., Hironaka, K.-I., Habara, O., Morishita, Y. & Nishimura, T. A developmental checkpoint directs metabolic remodelling as a strategy against starvation in Drosophila. *Nat. Metab.* **2**, 1096–1112 (2020).

30. Yamada, T. *et al.* The role of glycogen in development and adult fitness in Drosophila. *Dev. Camb. Engl.* **146**, dev176149 (2019).

31. Ugrankar, R. *et al.* Drosophila Snazarus Regulates a Lipid Droplet Population at Plasma Membrane-Droplet Contacts in Adipocytes. *Dev. Cell* **50**, 557-572.e5 (2019).

32. D'Erchia, A. M., Tullo, A., Lefkimmiatis, K., Saccone, C. & Sbisà, E. The fatty acid synthase gene is a conserved p53 family target from worm to human. *Cell Cycle* **5**, 750–758 (2006).

33. Walls, S. M. *et al.* Ceramide-Protein Interactions Modulate Ceramide-Associated Lipotoxic Cardiomyopathy. *Cell Rep.* **22**, 2702–2715 (2018).

34. Miao, T. *et al.* Acetyl-CoA-mediated autoacetylation of fatty acid synthase as a metabolic switch of de novo lipogenesis in *Drosophila*. *Proc. Natl. Acad. Sci.* **119**, e2212220119 (2022).

35. Garrido, D. *et al.* Fatty Acid Synthase Cooperates with Glyoxalase 1 to Protect against Sugar Toxicity. *PLOS Genet.* **11**, e1004995 (2015).

36. Nässel, D. R., Liu, Y. & Luo, J. Insulin/IGF signaling and its regulation in Drosophila. *Gen. Comp. Endocrinol.* **221**, 255–266 (2015).

37. Saltiel, A. R. Insulin signaling in health and disease. *J. Clin. Invest.* **131**, e142241, 142241 (2021).

38. Grewal, S. S. Insulin/TOR signaling in growth and homeostasis: a view from the fly world. *Int. J. Biochem. Cell Biol.* **41**, 1006–1010 (2009).

39. González, A., Hall, M. N., Lin, S.-C. & Hardie, D. G. AMPK and TOR: The Yin and Yang of Cellular Nutrient Sensing and Growth Control. *Cell Metab.* **31**, 472–492 (2020).

40. Hardie, D. G. AMP-Activated Protein Kinase: A Master Switch in Glucose and Lipid Metabolism. *Rev. Endocr. Metab. Disord.* **5**, 119–125 (2004).

41. Kunte, A. S., Matthews, K. A. & Rawson, R. B. Fatty acid auxotrophy in Drosophila larvae lacking SREBP. *Cell Metab.* **3**, 439–448 (2006).

42. Shao, W. & Espenshade, P. J. Expanding Roles for SREBP in Metabolism. *Cell Metab.* **16**, 414–419 (2012).

43. Porstmann, T. *et al.* SREBP Activity Is Regulated by mTORC1 and Contributes to Akt-Dependent Cell Growth. *Cell Metab.* **8**, 224–236 (2008).

44. Heier, C. & Kühnlein, R. P. Triacylglycerol Metabolism in Drosophila melanogaster. *Genetics* **210**, 1163–1184 (2018).

45. Suh, J. M. *et al.* Hedgehog signaling plays a conserved role in inhibiting fat formation. *Cell Metab.* **3**, 25–34 (2006).

46. Ugrankar, R. *et al.* Drosophila Snazarus Regulates a Lipid Droplet Population at Plasma Membrane-Droplet Contacts in Adipocytes. *Dev. Cell* **50**, 557-572.e5 (2019).

47. Kühnlein, R. P. Thematic review series: Lipid droplet synthesis and metabolism: from yeast to man. Lipid droplet-based storage fat metabolism in Drosophila. *J. Lipid Res.* **53**, 1430–1436 (2012).

48. Klepsatel, P., Knoblochová, D., Girish, T. N., Dircksen, H. & Gáliková, M. The influence of developmental diet on reproduction and metabolism in Drosophila. *BMC Evol. Biol.* **20**, 93 (2020).

49. Lanet, E. & Maurange, C. Building a brain under nutritional restriction: insights on sparing and plasticity from Drosophila studies. *Front. Physiol.* **5**, 117 (2014).

50. Avilés-Pagán, E. E. & Orr-Weaver, T. L. Activating embryonic development in Drosophila. *Semin. Cell Dev. Biol.* **84**, 100–110 (2018).

51. Welte, M. A. As the fat flies: The dynamic lipid droplets of Drosophila embryos. *Biochim. Biophys. Acta* **1851**, 1156–1185 (2015).

52. Sieber, M. H. & Spradling, A. C. Steroid Signaling Establishes a Female Metabolic State and Regulates SREBP to Control Oocyte Lipid Accumulation. *Curr. Biol.* **25**, 993–1004 (2015).

53. Ziegler, R. & Van Antwerpen, R. Lipid uptake by insect oocytes. *Insect Biochem. Mol. Biol.* **36**, 264–272 (2006).

54. Buch, S., Melcher, C., Bauer, M., Katzenberger, J. & Pankratz, M. J. Opposing effects of dietary protein and sugar regulate a transcriptional target of Drosophila insulin-like peptide signaling. *Cell Metab.* **7**, 321–332 (2008).

55. Rulifson, E. Fly-let biology and the high protein/low carb diet. *Cell Metab.* **7**, 281–283 (2008).

56. Kilwein, M. D., Johnson, M. R., Thomalla, J. M., Mahowald, A. P. & Welte, M. A. Drosophila embryos spatially sort their nutrient stores to facilitate their utilization. *Dev. Camb. Engl.* **150**, dev201423 (2023).

57. Yamada, T., Habara, O., Kubo, H. & Nishimura, T. Fat body glycogen serves as a metabolic safeguard for the maintenance of sugar levels in *Drosophila*. *Development* **145**, dev158865 (2018).

58. Arce-Molina, R. *et al.* A highly responsive pyruvate sensor reveals pathway-regulatory role of the mitochondrial pyruvate carrier MPC. *eLife* **9**, e53917 (2020).

59. Lee, J. E., Oney, M., Frizzell, K., Phadnis, N. & Hollien, J. Drosophila melanogaster activating transcription factor 4 regulates glycolysis during endoplasmic reticulum stress. *G3 Bethesda Md* **5**, 667–675 (2015).

60. Mengmeng Liu *et al.* Wingless signaling promotes lipid mobilization through signal-induced transcriptional repression. *bioRxiv* 2023.01.25.525602 (2023) doi:10.1101/2023.01.25.525602.

61. Williams, N. C. & O'Neill, L. A. J. A Role for the Krebs Cycle Intermediate Citrate in Metabolic Reprogramming in Innate Immunity and Inflammation. *Front. Immunol.* **9**, 141 (2018).

62. Liu, X., Qiao, Y., Ting, X. & Si, W. Isocitrate dehydrogenase 3A, a rate-limiting enzyme of the TCA cycle, promotes hepatocellular carcinoma migration and invasion through regulation of MTA1, a core component of the NuRD complex.

63. Sarkar, S., Chang, C.-I., Jean, J. & Wu, M.-J. TCA cycle-derived oncometabolites in cancer and the immune microenvironment. *J. Biomed. Sci.* **32**, 87 (2025).

64. Martínez-Reyes, I. & Chandel, N. S. Mitochondrial TCA cycle metabolites control physiology and disease. *Nat. Commun.* **11**, 102 (2020).

65. Ugrankar-Banerjee, R. *et al.* The fat body cortical actin network regulates Drosophila inter-organ nutrient trafficking, signaling, and adipose cell size. *eLife* **12**, e81170 (2023).

66. Ugrankar, R. *et al.* Drosophila glucome screening identifies Ck1alpha as a regulator of mammalian glucose metabolism. *Nat. Commun.* **6**, 7102 (2015).

67. Heier, C. & Kühnlein, R. P. Triacylglycerol Metabolism in *Drosophila melanogaster*. *Genetics* **210**, 1163–1184 (2018).

68. da Silva, G. F. *et al.* Assessing the Effects of Palm Oil Consumption on Life Expectancy, Metabolic Markers, and Oxidative Stress in Drosophila melanogaster. *Cell Biochem. Funct.* **42**, e70017 (2024).

69. Sung, Y., Yu, Y. C. & Han, J. M. Nutrient sensors and their crosstalk. *Exp. Mol. Med.* **55**, 1076–1089 (2023).

70. Bo, T. *et al.* Hepatic selective insulin resistance at the intersection of insulin signaling and metabolic dysfunction-associated steatotic liver disease. *Cell Metab.* **36**, 947–968 (2024).

71. Baker, K. D. & Thummel, C. S. Diabetic Larvae and Obese Flies—Emerging Studies of Metabolism in Drosophila. *Cell Metab.* **6**, 257–266 (2007).

72. Steinberg, G. R. & Hardie, D. G. New insights into activation and function of the AMPK. *Nat. Rev. Mol. Cell Biol.* **24**, 255–272 (2023).

73. Ashe, K. M. *et al.* Inhibition of glycogen biosynthesis via mTORC1 suppression as an adjunct therapy for Pompe disease. *Mol. Genet. Metab.* **100**, 309–315 (2010).

74. Ruiz, R. *et al.* Sterol Regulatory Element-binding Protein-1 (SREBP-1) Is Required to Regulate Glycogen Synthesis and Gluconeogenic Gene Expression in Mouse Liver. *J. Biol. Chem.* **289**, 5510–5517 (2014).

75. Williams, N. C. & O'Neill, L. A. J. A Role for the Krebs Cycle Intermediate Citrate in Metabolic Reprogramming in Innate Immunity and Inflammation. *Front. Immunol.* **9**, 141 (2018).

76. Musumeci, O. *et al.* Clinical features and new molecular findings in muscle phosphofructokinase deficiency (GSD type VII). *Neuromuscul. Disord. NMD* **22**, 325–330 (2012).

77. Xu, X. *et al.* Insulin Signaling Regulates Fatty Acid Catabolism at the Level of CoA Activation. *PLoS Genet.* **8**, e1002478 (2012).

78. Dobrosotskaya, I. Y., Seegmiller, A. C., Brown, M. S., Goldstein, J. L. & Rawson, R. B. Regulation of SREBP Processing and Membrane Lipid Production by Phospholipids in *Drosophila*. *Science* **296**, 879–883 (2002).

79. Shi, L. & Tu, B. P. Acetyl-CoA and the regulation of metabolism: mechanisms and consequences. *Curr. Opin. Cell Biol.* **33**, 125–131 (2015).

80. Wang, Y. *et al.* The multiple facets of acetyl-CoA metabolism: Energetics, biosynthesis, regulation, acylation and inborn errors. *Mol. Genet. Metab.* **138**, 106966 (2023).

81. Bradshaw, P. C. Acetyl-CoA Metabolism and Histone Acetylation in the Regulation of Aging and Lifespan. *Antioxidants* **10**, 572 (2021).

82. Giandomenico, V., Simonsson, M., Grünroos, E. & Ericsson, J. Coactivator-Dependent Acetylation Stabilizes Members of the SREBP Family of Transcription Factors. *Mol. Cell. Biol.* **23**, 2587–2599 (2003).

83. Sivanand, S., Viney, I. & Wellen, K. E. Spatiotemporal Control of Acetyl-CoA Metabolism in Chromatin Regulation. *Trends Biochem. Sci.* **43**, 61–74 (2018).

84. Mews, P. *et al.* Acetyl-CoA synthetase regulates histone acetylation and hippocampal memory. *Nature* **546**, 381–386 (2017).

85. Park, J.-M., Jo, S.-H., Kim, M.-Y., Kim, T.-H. & Ahn, Y.-H. Role of transcription factor acetylation in the regulation of metabolic homeostasis. *Protein Cell* **6**, 804–813 (2015).

86. Schirling, C. *et al.* Widespread regulation of gene expression in the Drosophila genome by the histone acetyltransferase dTip60. *Chromosoma* **119**, 99–113 (2010).

87. Boros, I. M. Histone modification in Drosophila. *Brief. Funct. Genomics* **11**, 319–331 (2012).

88. Seegmiller, A. C. *et al.* The SREBP pathway in Drosophila: regulation by palmitate, not sterols. *Dev. Cell* **2**, 229–238 (2002).

89. Marsh, A. J. *et al.* Catalytic-dependent and independent functions of the histone acetyltransferase CBP promote pioneer factor-mediated zygotic genome activation. Preprint at https://doi.org/10.1101/2024.10.04.616638 (2024).

90. Koval, L. A. *et al.* [Drosophila melanogaster Lifespan Is Regulated by nejire Gene Expression in Peripheral Tissues and Nervous System]. *Mol. Biol. (Mosk.)* **57**, 833–852 (2023).

91. Santopietro, M. V., Ferreri, D., Prozzillo, Y., Dimitri, P. & Messina, G. The multitalented TIP60 chromatin remodeling complex: wearing many hats in epigenetic regulation, cell division and diseases. *Epigenetics Chromatin* **18**, 40 (2025).

92. Xiao, Y. *et al.* Dynamic interactions between TIP60 and p300 regulate FOXP3 function through a structural switch defined by a single lysine on TIP60. *Cell Rep.* **7**, 1471–1480 (2014).

93. Galdieri, L. & Vancura, A. Acetyl-CoA carboxylase regulates global histone acetylation. *J. Biol. Chem.* **287**, 23865–23876 (2012).

94. Morciano, P. *et al.* Depletion of ATP-Citrate Lyase (ATPCL) Affects Chromosome Integrity Without Altering Histone Acetylation in Drosophila Mitotic Cells. *Front. Physiol.* **10**, 383 (2019).

95. Gefen, E., Marlon, A. J. & Gibbs, A. G. Selection for desiccation resistance in adult Drosophila melanogaster affects larval development and metabolite accumulation. *J. Exp. Biol.* **209**, 3293–3300 (2006).

96. Tsuyama, T., Hayashi, Y., Komai, H., Shimono, K. & Uemura, T. Dynamic de novo adipose tissue development during metamorphosis in Drosophila melanogaster. *Development* **150**, dev200815 (2023).

97. Lei, Y. *et al.* FGF signaling promotes spreading of fat body precursors necessary for adult adipogenesis in Drosophila. *PLoS Biol.* **21**, e3002050 (2023).

98. Parra-Peralbo, E. & Culi, J. Drosophila lipophorin receptors mediate the uptake of neutral lipids in oocytes and imaginal disc cells by an endocytosis-independent mechanism. *PLoS Genet.* **7**, e1001297 (2011).

99. Buszczak, M., Lu, X., Segraves, W. A., Chang, T. Y. & Cooley, L. Mutations in the midway gene disrupt a Drosophila acyl coenzyme A: diacylglycerol acyltransferase. *Genetics* **160**, 1511–1518 (2002).

100. Chitraju, C., Fischer, A. W., Farese, R. V. & Walther, T. C. Lipid Droplets in Brown Adipose Tissue Are Dispensable for Cold-Induced Thermogenesis. *Cell Rep.* **33**, 108348 (2020).

101. White, R. P. & Welte, M. A. Visualizing Lipid Droplets in Drosophila Oogenesis. *Methods Mol. Biol.* **2626**, 233–251 (2023).

102. Avilés-Pagán, E. E. & Orr-Weaver, T. L. Activating embryonic development in Drosophila. *Semin. Cell Dev. Biol.* **84**, 100–110 (2018).

103. Welte, M. A. As the fat flies: The dynamic lipid droplets of Drosophila embryos. *Biochim. Biophys. Acta BBA - Mol. Cell Biol. Lipids* **1851**, 1156–1185 (2015).

104. Aurora, A. B. *et al.* Loss of glucose 6-phosphate dehydrogenase function increases oxidative stress and glutaminolysis in metastasizing melanoma cells. *Proc. Natl. Acad. Sci. U. S. A.* **119**, e2120617119 (2022).

105. Tasdogan, A. *et al.* Metabolic heterogeneity confers differences in melanoma metastatic potential. *Nature* **577**, 115–120 (2020).

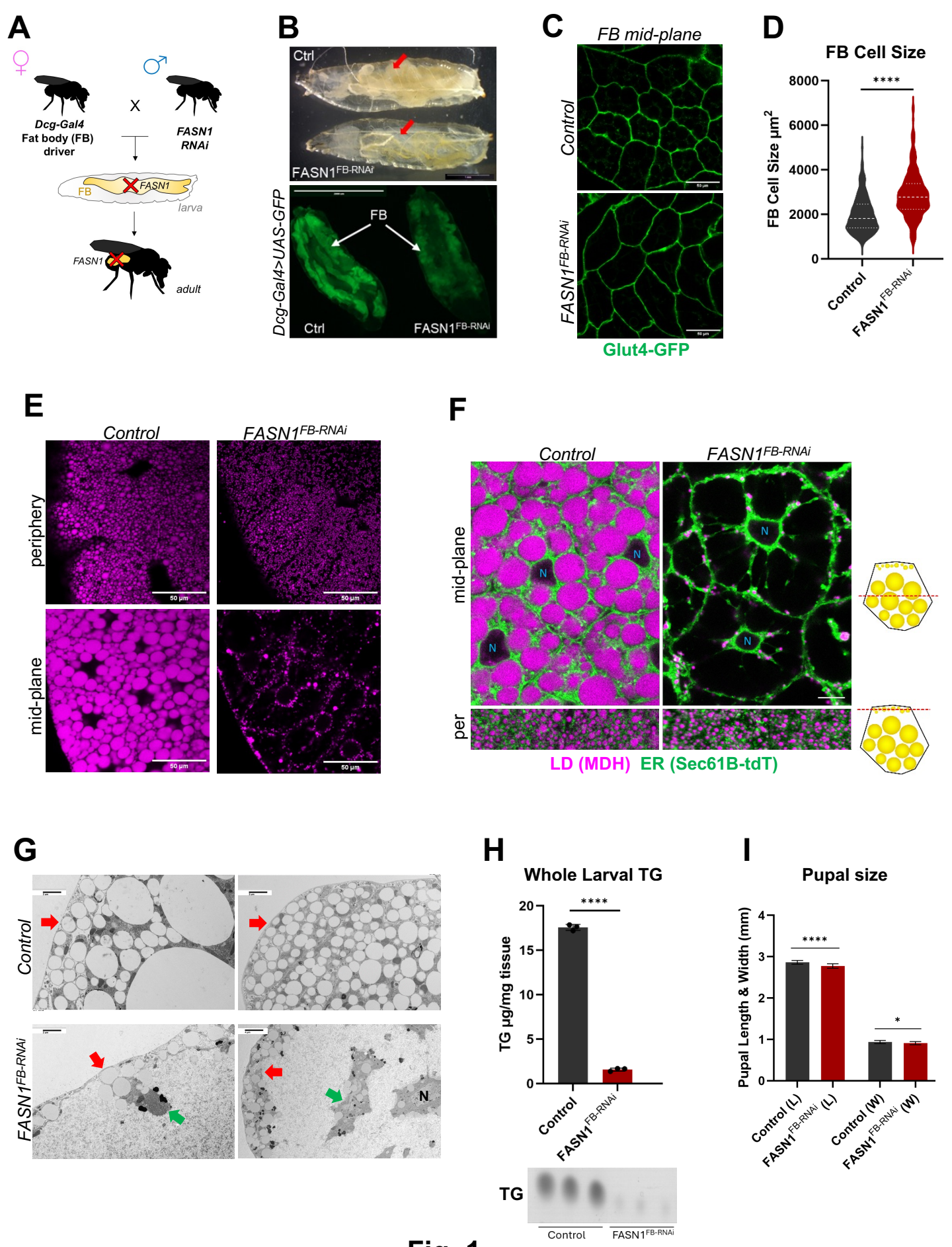
A
Dcg-Gal4
Fat body (FB)
driver
X
FASN1
RNAi
FB
FASN1
larva
FASN1
adult
B
Ctrl
FASN1FB-RNAi
Dcg-Gal4>UAS-GFP
FB
Ctrl
FASN1FB-RNAi
C
FB mid-plane
Control
FASN1FB-RNAi
Glut4-GFP
D
FB Cell Size
FB Cell Size µm2
8000
6000
4000
2000
0
****
Control
FASN1FB-RNAi
E
Control
FASN1FB-RNAi
periphery
mid-plane
50 µm
F
Control
FASN1FB-RNAi
mid-plane
per
N
LD (MDH) ER (Sec61B-tdT)
G
Control
FASN1FB-RNAi
N
H
Whole Larval TG
TG µg/mg tissue
20
15
10
5
0
****
Control
FASN1FB-RNAi
TG
Control
FASN1FB-RNAi
I
Pupal size
Pupal Length & Width (mm)
4
3
2
1
0
****
*
Control (L)
FASN1FB-RNAi (L)
Control (W)
FASN1FB-RNAi (W)

Fig. 1

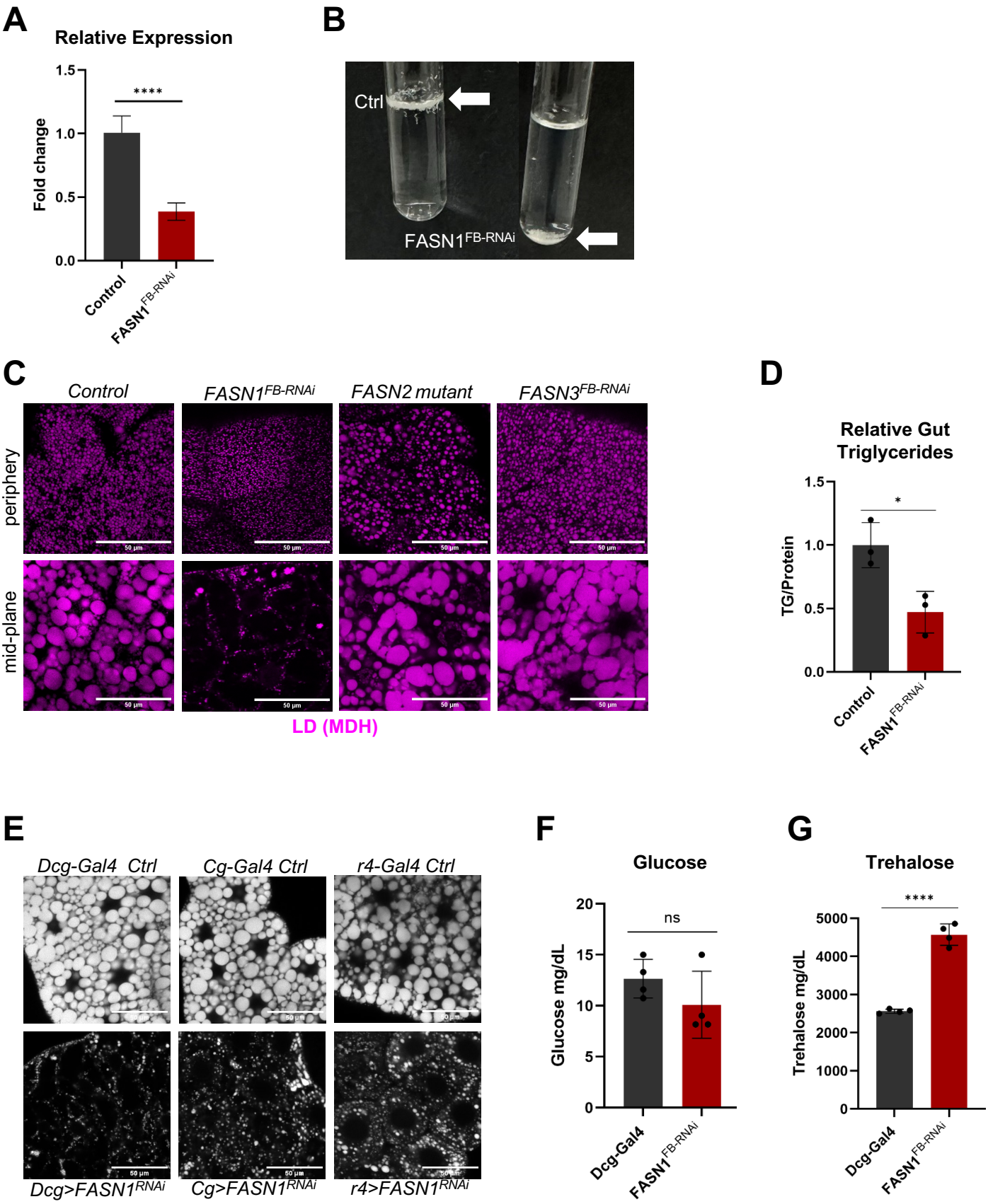
A
Relative Expression
Fold change
1.5
1.0
0.5
0.0
****
Control
FASN1FB-RNAi
B
Ctrl
FASN1FB-RNAi
C
Control
FASN1FB-RNAi
FASN2 mutant
FASN3FB-RNAi
periphery
mid-plane
50 µm
LD (MDH)
D
Relative Gut Triglycerides
TG/Protein
1.5
1.0
0.5
0.0
*
Control
FASN1FB-RNAi
E
Dcg-Gal4 Ctrl
Cg-Gal4 Ctrl
r4-Gal4 Ctrl
Dcg>FASN1RNAi
Cg>FASN1RNAi
r4>FASN1RNAi
F
Glucose
Glucose mg/dL
20
15
10
5
0
ns
Dcg-Gal4
FASN1FB-RNAi
G
Trehalose
Trehalose mg/dL
5000
4000
3000
2000
1000
0
****
Dcg-Gal4
FASN1FB-RNAi

Supp Fig. 1

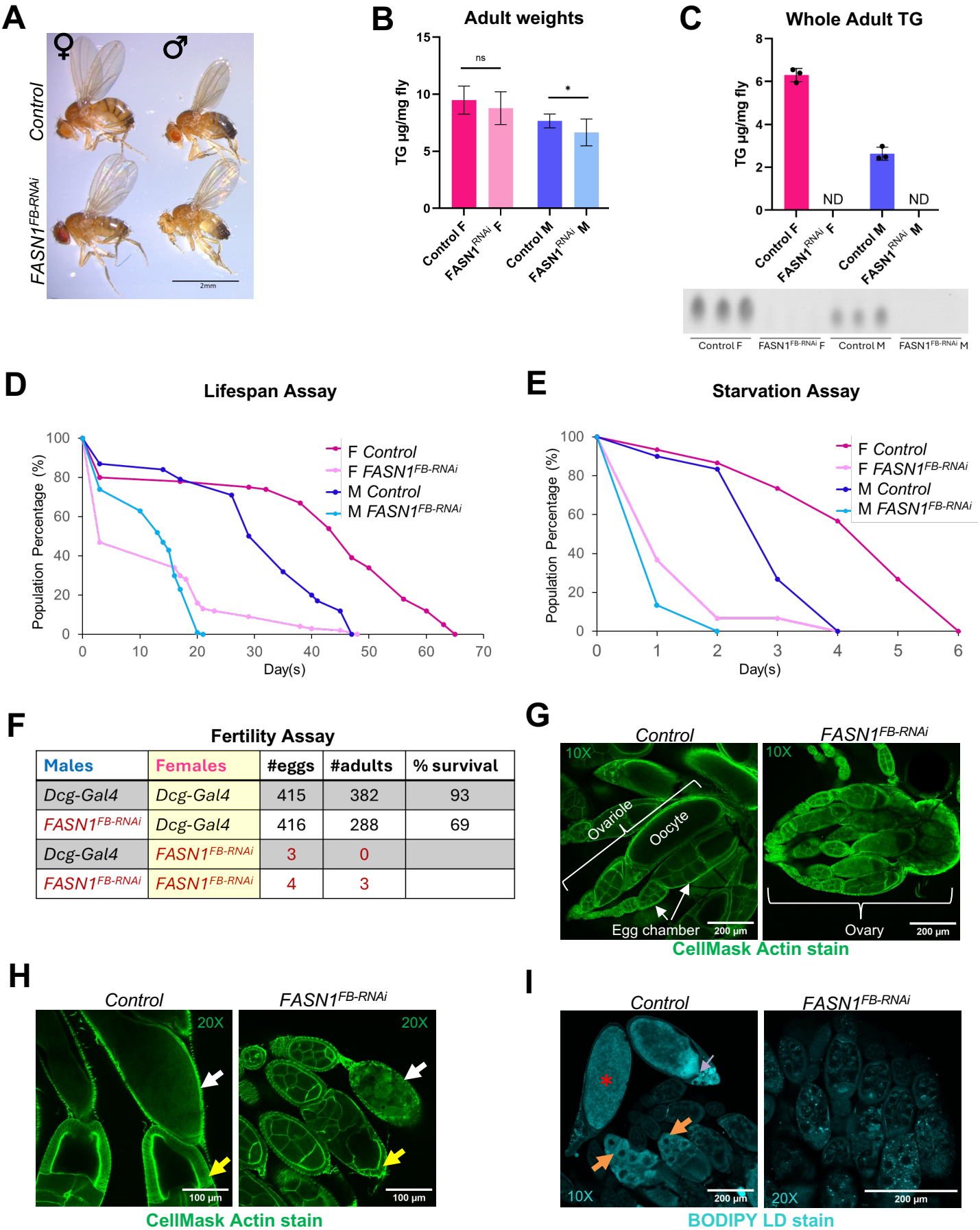

Males	Females	#eggs	#adults	% survival
Dcg-Gal4	*Dcg-Gal4*	415	382	93
FASN1FB-RNAi	*Dcg-Gal4*	416	288	69
Dcg-Gal4	*FASN1FB-RNAi*	3	0	
FASN1FB-RNAi	*FASN1FB-RNAi*	4	3	

Fig. 2

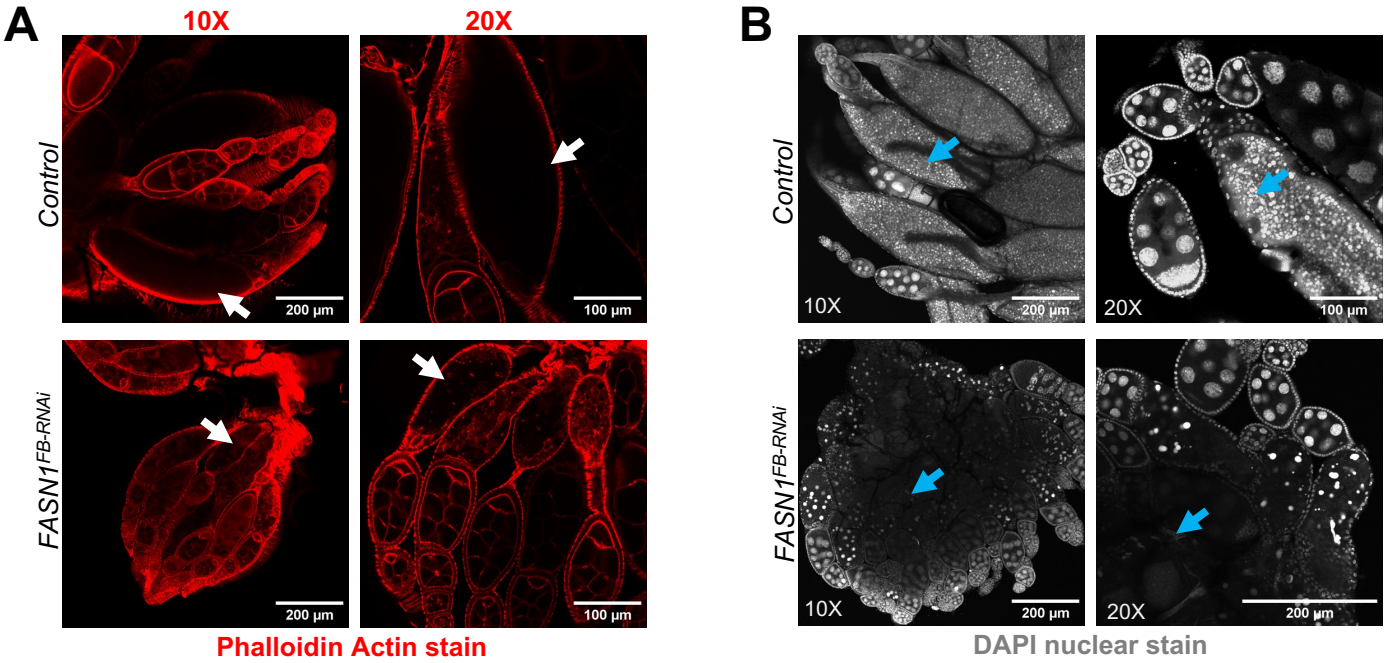
A
10X
20X
Control
FASN1FB-RNAi
200 µm
100 µm
Phalloidin Actin stain
B
Control
FASN1FB-RNAi
10X
20X
200 µm
100 µm
DAPI nuclear stain

Supp Fig. 2

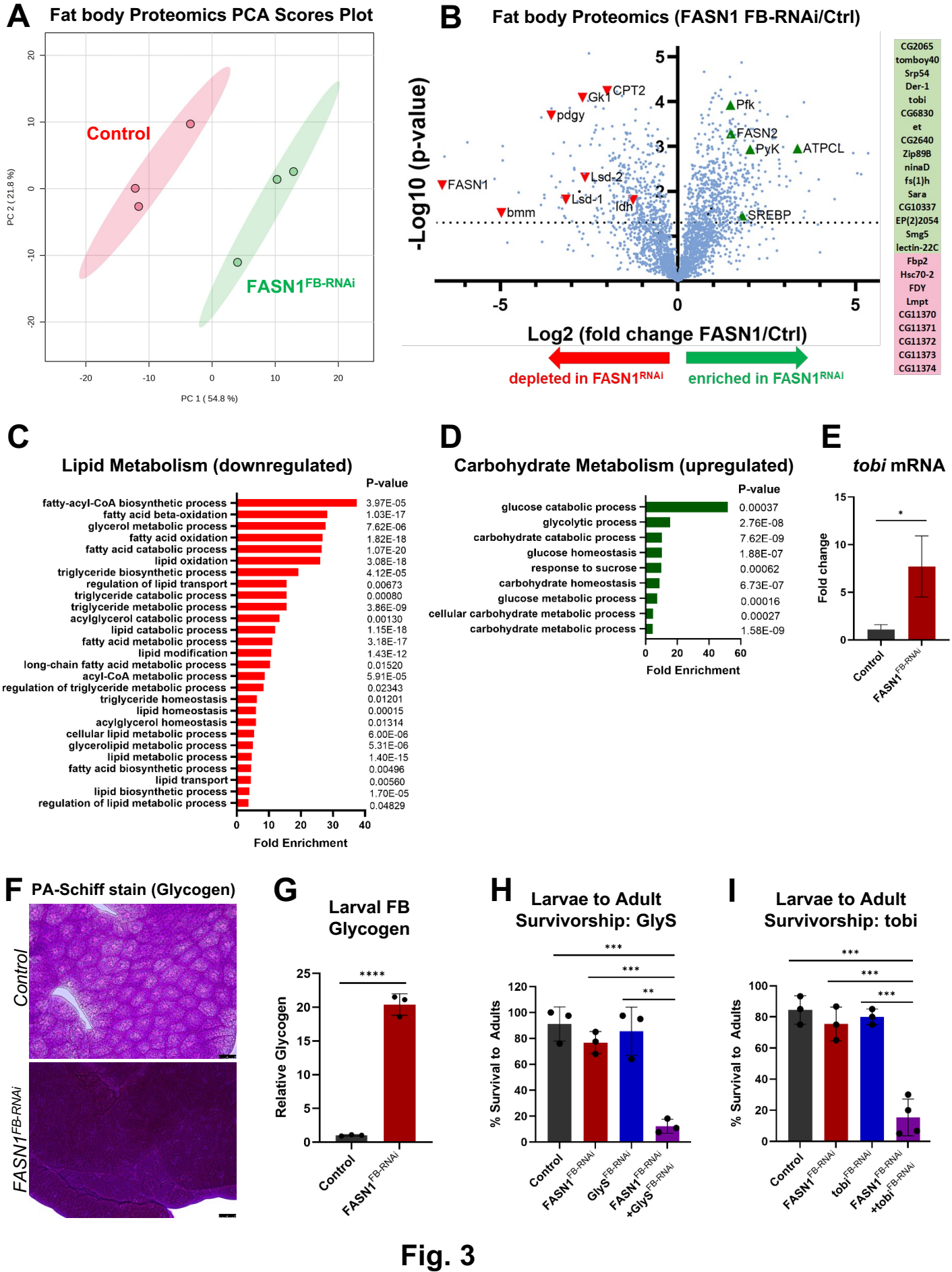
A
Fat body Proteomics PCA Scores Plot
Control
FASN1FB-RNAi
PC 2 (21.8 %)
PC 1 (54.8 %)
B
Fat body Proteomics (FASN1 FB-RNAi/Ctrl)
-Log10 (p-value)
Log2 (fold change FASN1/Ctrl)
depleted in FASN1RNAi
enriched in FASN1RNAi
CPT2
Gk1
pdgy
Pfk
FASN2
PyK
ATPCL
FASN1
Lsd-2
Lsd-1
Idh
bmm
SREBP
CG2065
tomboy40
Srp54
Der-1
tobi
CG6830
et
CG2640
Zip89B
ninaD
fs(1)h
Sara
CG10337
EP(2)2054
Smg5
lectin-22C
Fbp2
Hsc70-2
FDY
Lmpt
CG11370
CG11371
CG11372
CG11373
CG11374
C
Lipid Metabolism (downregulated)
P-value
fatty-acyl-CoA biosynthetic process 3.97E-05
fatty acid beta-oxidation 1.03E-17
glycerol metabolic process 7.62E-06
fatty acid oxidation 1.82E-18
fatty acid catabolic process 1.07E-20
lipid oxidation 3.08E-18
triglyceride biosynthetic process 4.12E-05
regulation of lipid transport 0.00673
triglyceride catabolic process 0.00080
triglyceride metabolic process 3.86E-09
acylglycerol catabolic process 0.00130
lipid catabolic process 1.15E-18
fatty acid metabolic process 3.18E-17
lipid modification 1.43E-12
long-chain fatty acid metabolic process 0.01520
acyl-CoA metabolic process 5.91E-05
regulation of triglyceride metabolic process 0.02343
triglyceride homeostasis 0.01201
lipid homeostasis 0.00015
acylglycerol homeostasis 0.01314
cellular lipid metabolic process 6.00E-06
glycerolipid metabolic process 5.31E-06
lipid metabolic process 1.40E-15
fatty acid biosynthetic process 0.00496
lipid transport 0.00560
lipid biosynthetic process 1.70E-05
regulation of lipid metabolic process 0.04829
Fold Enrichment
D
Carbohydrate Metabolism (upregulated)
P-value
glucose catabolic process 0.00037
glycolytic process 2.76E-08
carbohydrate catabolic process 7.62E-09
glucose homeostasis 1.88E-07
response to sucrose 0.00062
carbohydrate homeostasis 6.73E-07
glucose metabolic process 0.00016
cellular carbohydrate metabolic process 0.00027
carbohydrate metabolic process 1.58E-09
Fold Enrichment
E
tobi mRNA
Fold change
Control
FASN1FB-RNAi
F
PA-Schiff stain (Glycogen)
Control
FASN1FB-RNAi
G
Larval FB Glycogen
Relative Glycogen
Control
FASN1FB-RNAi
H
Larvae to Adult Survivorship: GlyS
% Survival to Adults
Control
FASN1FB-RNAi
GlySFB-RNAi
FASN1FB-RNAi +GlySFB-RNAi
I
Larvae to Adult Survivorship: tobi
% Survival to Adults
Control
FASN1FB-RNAi
tobiFB-RNAi
FASN1FB-RNAi +tobiFB-RNAi

Fig. 3

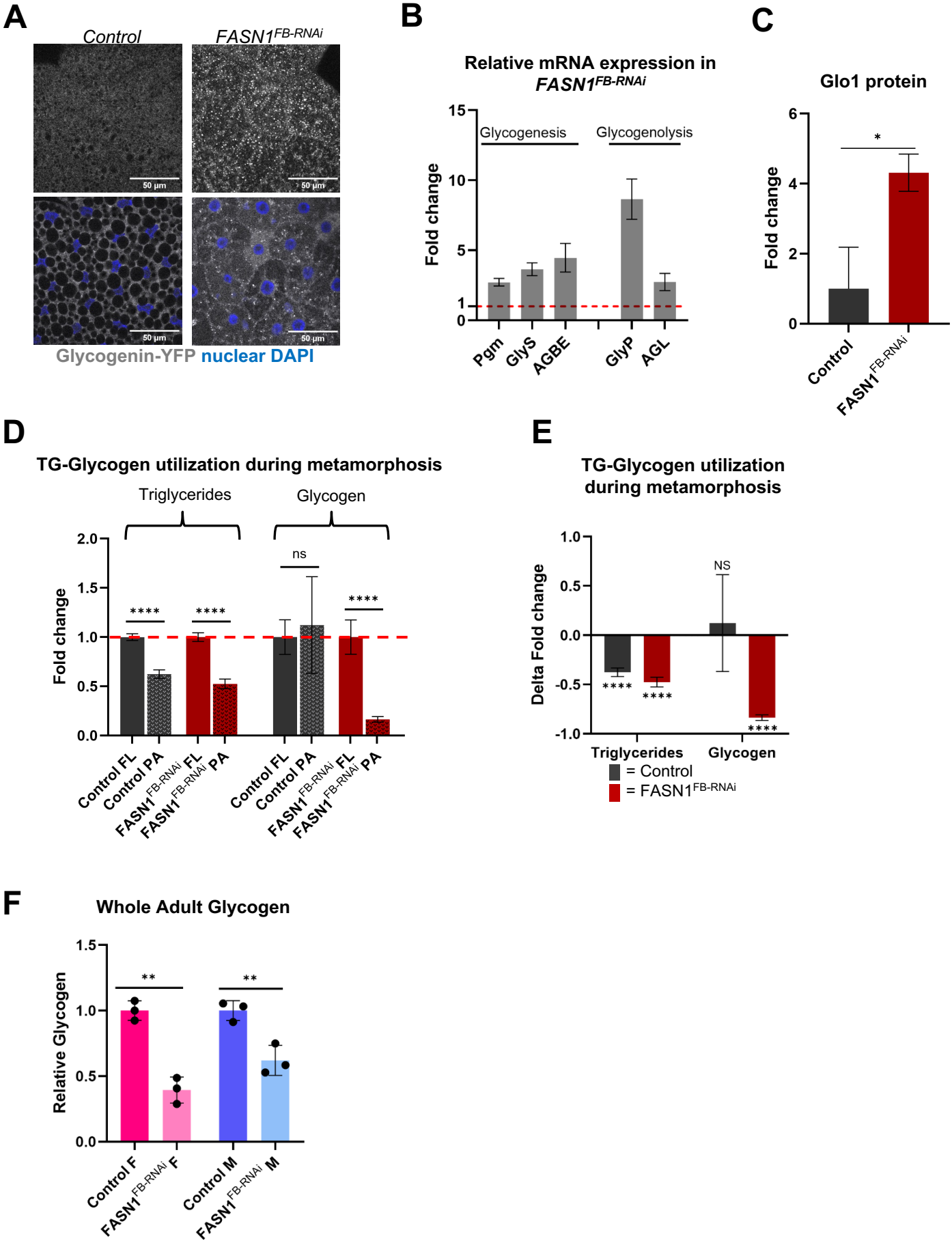
A
Control
FASN1FB-RNAi
50 µm
Glycogenin-YFP nuclear DAPI
B
Relative mRNA expression in FASN1FB-RNAi
Glycogenesis
Glycogenolysis
Fold change
Pgm
GlyS
AGBE
GlyP
AGL
C
Glo1 protein
Fold change
Control
FASN1FB-RNAi
D
TG-Glycogen utilization during metamorphosis
Triglycerides
Glycogen
Fold change
ns
Control FL
Control PA
FASN1FB-RNAi FL
FASN1FB-RNAi PA
E
TG-Glycogen utilization during metamorphosis
Delta Fold change
NS
Triglycerides
Glycogen
= Control
= FASN1FB-RNAi
F
Whole Adult Glycogen
Relative Glycogen
Control F
FASN1FB-RNAi F
Control M
FASN1FB-RNAi M

Supp Fig. 3

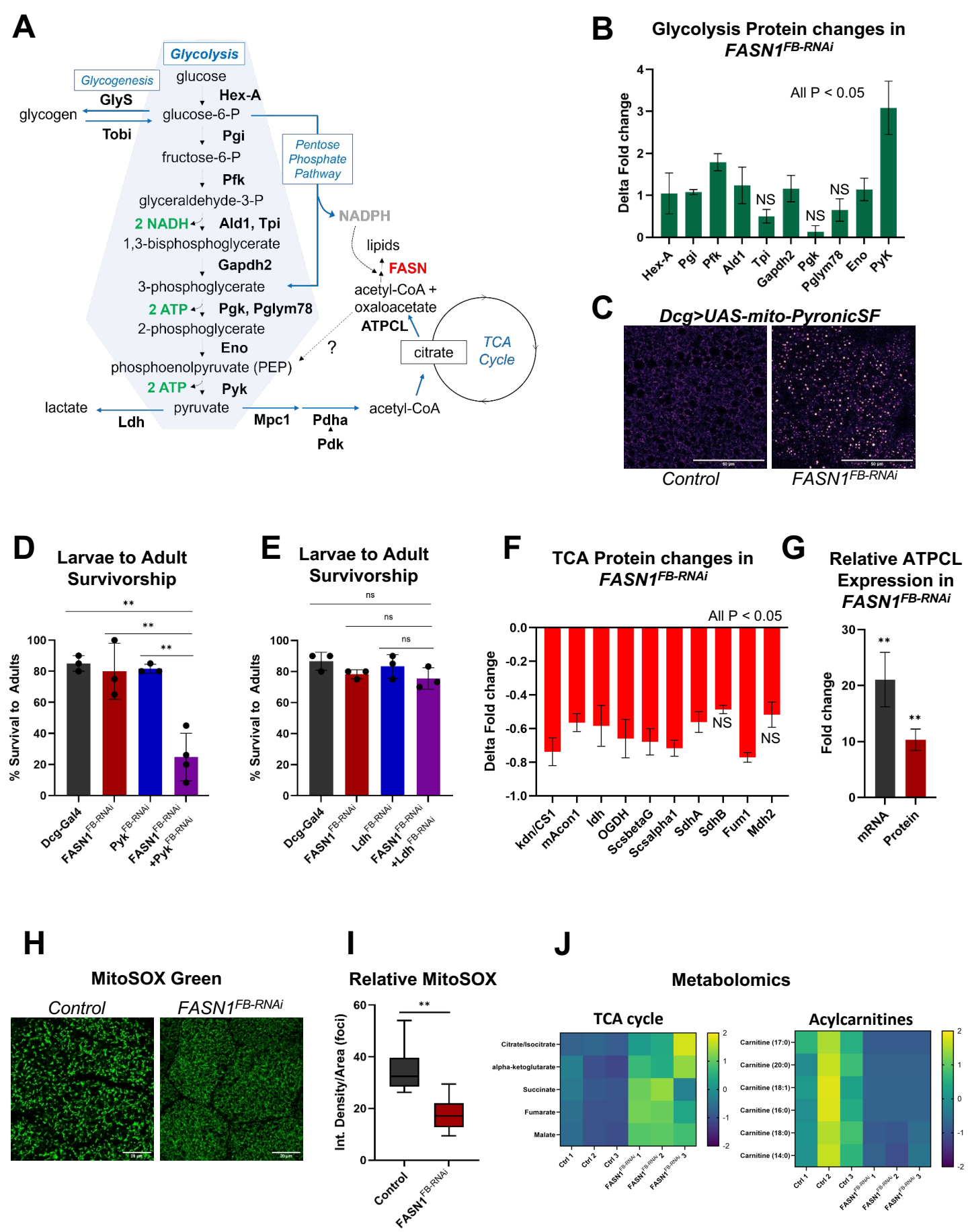
A
Glycolysis
Glycogenesis
glucose
GlyS
Hex-A
glycogen
glucose-6-P
Tobi
Pgi
fructose-6-P
Pentose Phosphate Pathway
Pfk
glyceraldehyde-3-P
NADPH
2 NADH
Ald1, Tpi
1,3-bisphosphoglycerate
lipids
FASN
Gapdh2
3-phosphoglycerate
acetyl-CoA +
oxaloacetate
2 ATP
Pgk, Pglym78
ATPCL
2-phosphoglycerate
Eno
?
citrate
TCA Cycle
phosphoenolpyruvate (PEP)
2 ATP
Pyk
lactate
pyruvate
acetyl-CoA
Ldh
Mpc1
Pdha
Pdk
B
Glycolysis Protein changes in FASN1FB-RNAi
All P < 0.05
Delta Fold change
NS
Hex-A
Pgi
Pfk
Ald1
Tpi
Gapdh2
Pgk
Pglym78
Eno
PyK
C
Dcg>UAS-mito-PyronicSF
Control
FASN1FB-RNAi
D
Larvae to Adult Survivorship
% Survival to Adults
Dcg-Gal4
FASN1FB-RNAi
PykFB-RNAi
FASN1FB-RNAi +PykFB-RNAi
E
Larvae to Adult Survivorship
% Survival to Adults
ns
Dcg-Gal4
FASN1FB-RNAi
LdhFB-RNAi
FASN1FB-RNAi +LdhFB-RNAi
F
TCA Protein changes in FASN1FB-RNAi
All P < 0.05
Delta Fold change
NS
kdn/CS1
mAcon1
Idh
OGDH
ScsbetaG
Scsalpha1
SdhA
SdhB
Fum1
Mdh2
G
Relative ATPCL Expression in FASN1FB-RNAi
Fold change
mRNA
Protein
H
MitoSOX Green
Control
FASN1FB-RNAi
I
Relative MitoSOX
Int. Density/Area (foci)
Control
FASN1FB-RNAi
J
Metabolomics
TCA cycle
Citrate/Isocitrate
alpha-ketoglutarate
Succinate
Fumarate
Malate
Acylcarnitines
Carnitine (17:0)
Carnitine (20:0)
Carnitine (18:1)
Carnitine (16:0)
Carnitine (18:0)
Carnitine (14:0)

Fig. 4

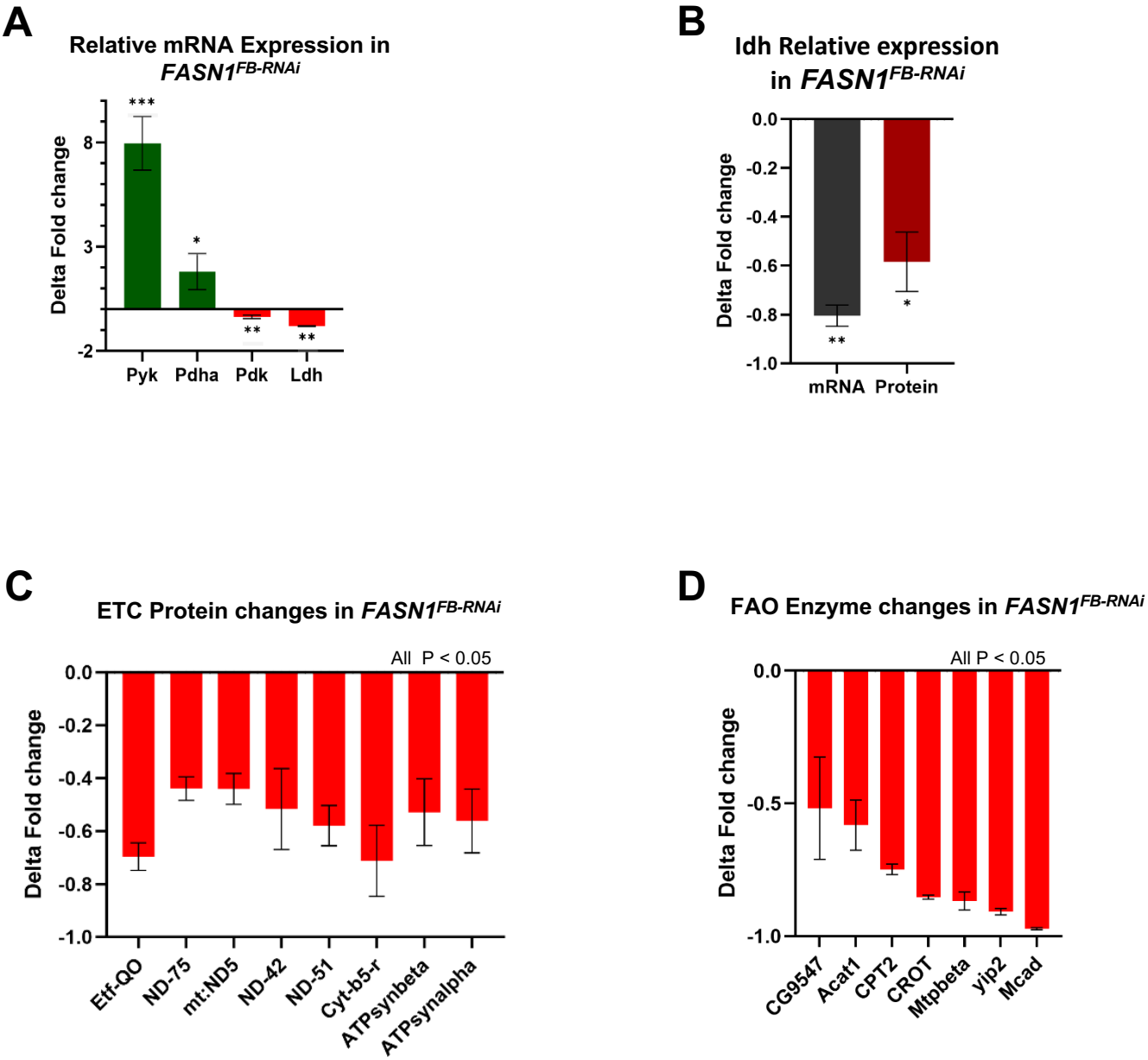
A
Relative mRNA Expression in FASN1FB-RNAi
Delta Fold change
8
3
-2
***
*
**
**
Pyk
Pdha
Pdk
Ldh
B
Idh Relative expression in FASN1FB-RNAi
Delta Fold change
0.0
-0.2
-0.4
-0.6
-0.8
-1.0
**
*
mRNA
Protein
C
ETC Protein changes in FASN1FB-RNAi
All P < 0.05
Delta Fold change
0.0
-0.2
-0.4
-0.6
-0.8
-1.0
Etf-QO
ND-75
mt:ND5
ND-42
ND-51
Cyt-b5-r
ATPsynbeta
ATPsynalpha
D
FAO Enzyme changes in FASN1FB-RNAi
All P < 0.05
Delta Fold change
0.0
-0.5
-1.0
CG9547
Acat1
CPT2
CROT
Mtpbeta
yip2
Mcad

Supp Fig. 4

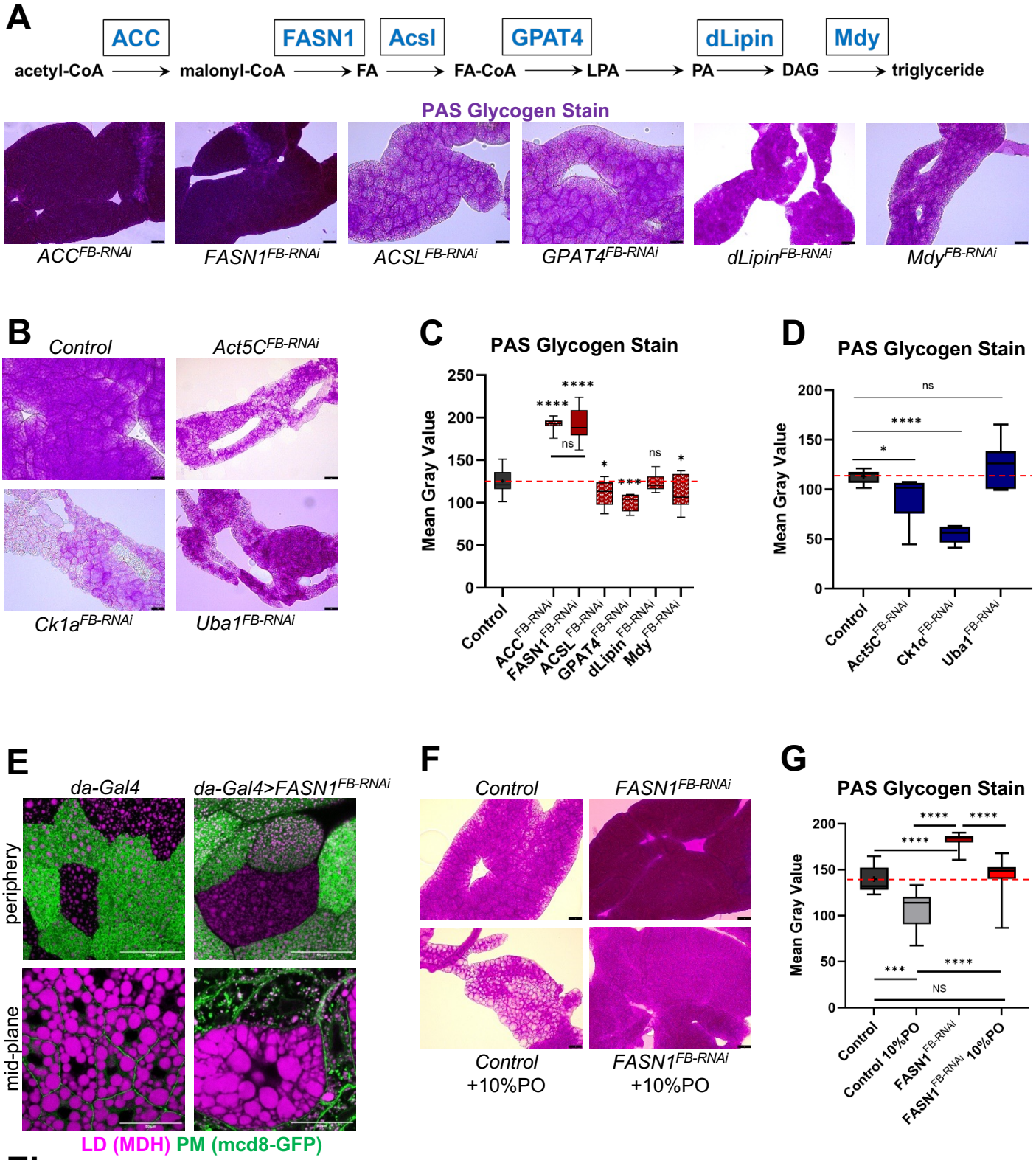
A
ACC
FASN1
Acsl
GPAT4
dLipin
Mdy
acetyl-CoA → malonyl-CoA → FA → FA-CoA → LPA → PA → DAG → triglyceride
PAS Glycogen Stain
ACC FB-RNAi
FASN1 FB-RNAi
ACSL FB-RNAi
GPAT4 FB-RNAi
dLipin FB-RNAi
Mdy FB-RNAi
B
Control
Act5C FB-RNAi
Ck1a FB-RNAi
Uba1 FB-RNAi
C
PAS Glycogen Stain
Mean Gray Value
250
200
150
100
50
0
****
****
ns
*
***
ns
*
Control
ACC FB-RNAi
FASN1 FB-RNAi
ACSL FB-RNAi
GPAT4 FB-RNAi
dLipin FB-RNAi
Mdy FB-RNAi
D
PAS Glycogen Stain
Mean Gray Value
200
150
100
50
0
ns
****
*
Control
Act5C FB-RNAi
Ck1α FB-RNAi
Uba1 FB-RNAi
E
da-Gal4
da-Gal4>FASN1 FB-RNAi
periphery
mid-plane
LD (MDH) PM (mcd8-GFP)
E'
da-Gal4 Ctrl
da-Gal4>FASN1 RNAi
F
Control
FASN1 FB-RNAi
Control +10%PO
FASN1 FB-RNAi +10%PO
G
PAS Glycogen Stain
Mean Gray Value
200
150
100
50
0
****
****
****
***
****
NS
Control
Control 10%PO
FASN1 FB-RNAi
FASN1 FB-RNAi 10%PO

Fig. 5

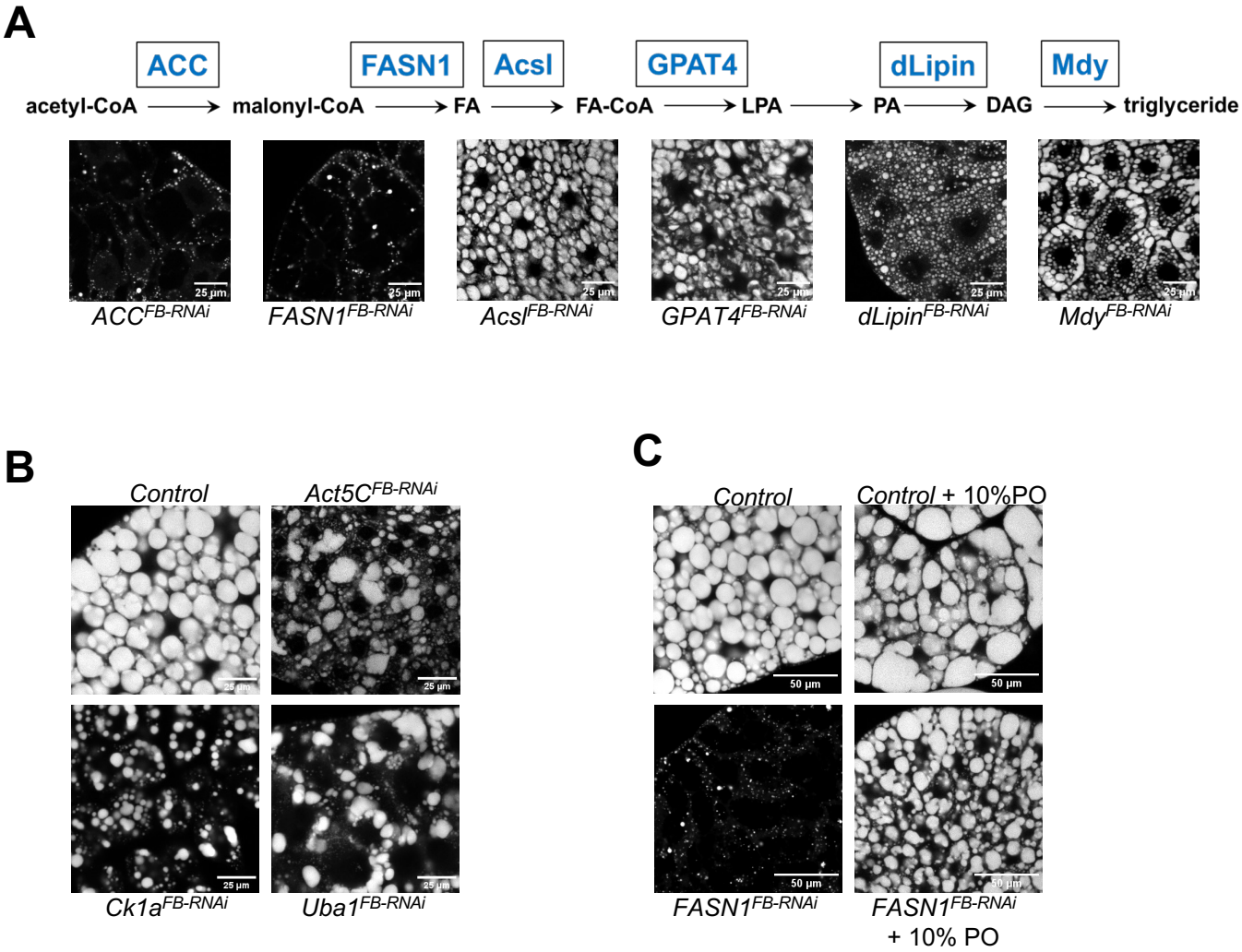
A
ACC
FASN1
Acsl
GPAT4
dLipin
Mdy
acetyl-CoA
malonyl-CoA
FA
FA-CoA
LPA
PA
DAG
triglyceride
ACC FB-RNAi
FASN1 FB-RNAi
Acsl FB-RNAi
GPAT4 FB-RNAi
dLipin FB-RNAi
Mdy FB-RNAi
B
Control
Act5C FB-RNAi
Ck1a FB-RNAi
Uba1 FB-RNAi
C
Control
Control + 10%PO
FASN1 FB-RNAi
FASN1 FB-RNAi + 10% PO

Supp Fig. 5

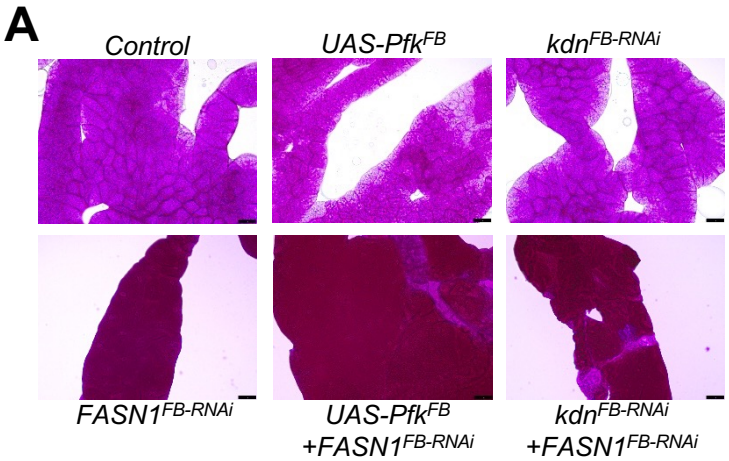
A
Control
UAS-Pfk^FB
kdn^FB-RNAi
FASN1^FB-RNAi
UAS-Pfk^FB +FASN1^FB-RNAi
kdn^FB-RNAi +FASN1^FB-RNAi

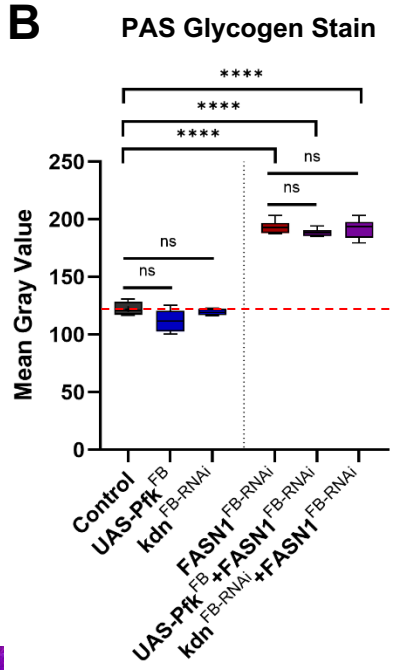
B
PAS Glycogen Stain
Mean Gray Value
250
200
150
100
50
0
****
****
****
ns
ns
ns
ns
Control
UAS-Pfk^FB
kdn^FB-RNAi
FASN1^FB-RNAi
UAS-Pfk^FB +FASN1^FB-RNAi
kdn^FB-RNAi +FASN1^FB-RNAi

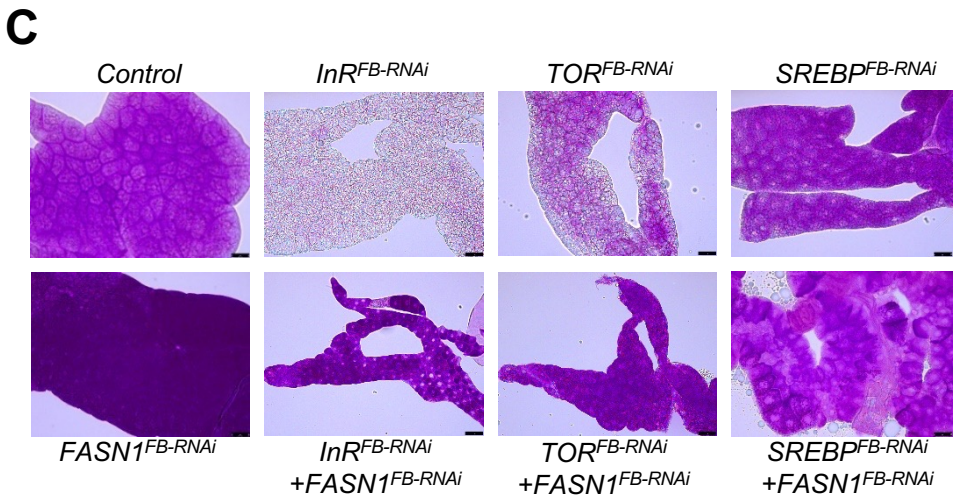
C
Control
InR^FB-RNAi
TOR^FB-RNAi
SREBP^FB-RNAi
FASN1^FB-RNAi
InR^FB-RNAi +FASN1^FB-RNAi
TOR^FB-RNAi +FASN1^FB-RNAi
SREBP^FB-RNAi +FASN1^FB-RNAi

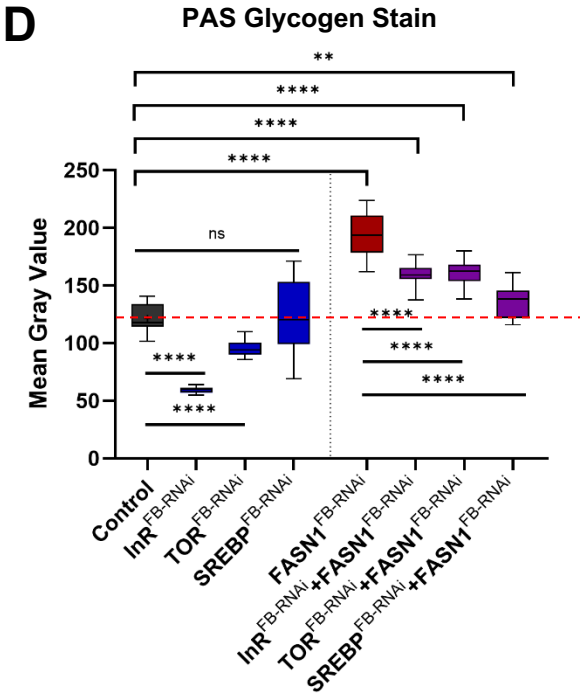
D
PAS Glycogen Stain
Mean Gray Value
250
200
150
100
50
0
**
****
****
****
ns
****
****
****
****
****
Control
InR^FB-RNAi
TOR^FB-RNAi
SREBP^FB-RNAi
FASN1^FB-RNAi
InR^FB-RNAi +FASN1^FB-RNAi
TOR^FB-RNAi +FASN1^FB-RNAi
SREBP^FB-RNAi +FASN1^FB-RNAi

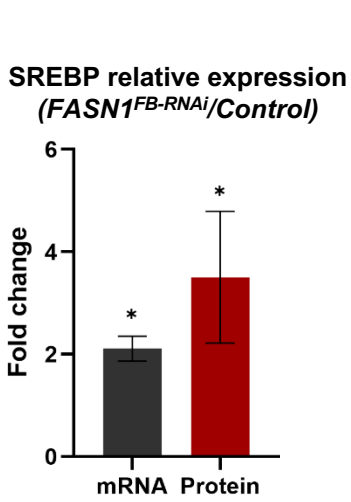
E
SREBP relative expression
(FASN1^FB-RNAi/Control)
Fold change
6
4
2
0
*
*
mRNA
Protein

Fig. 6

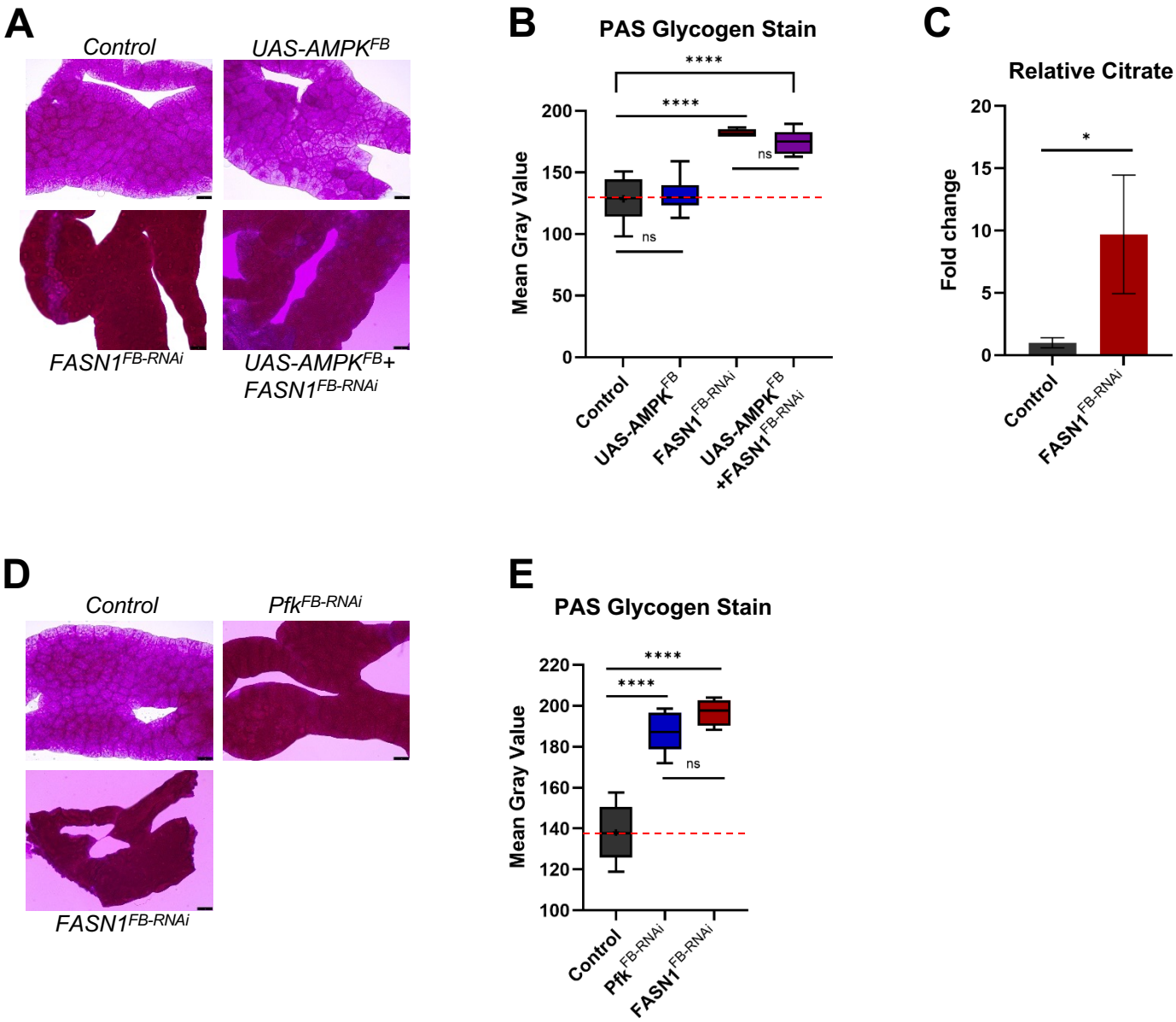
A
Control
UAS-AMPK^FB
FASN1^FB-RNAi
UAS-AMPK^FB+
FASN1^FB-RNAi
B
PAS Glycogen Stain
Mean Gray Value
****
****
ns
ns
Control
UAS-AMPK^FB
FASN1^FB-RNAi
UAS-AMPK^FB
+FASN1^FB-RNAi
C
Relative Citrate
Fold change
*
Control
FASN1^FB-RNAi
D
Control
Pfk^FB-RNAi
FASN1^FB-RNAi
E
PAS Glycogen Stain
Mean Gray Value
****
****
ns
Control
Pfk^FB-RNAi
FASN1^FB-RNAi

Supp Fig. 6

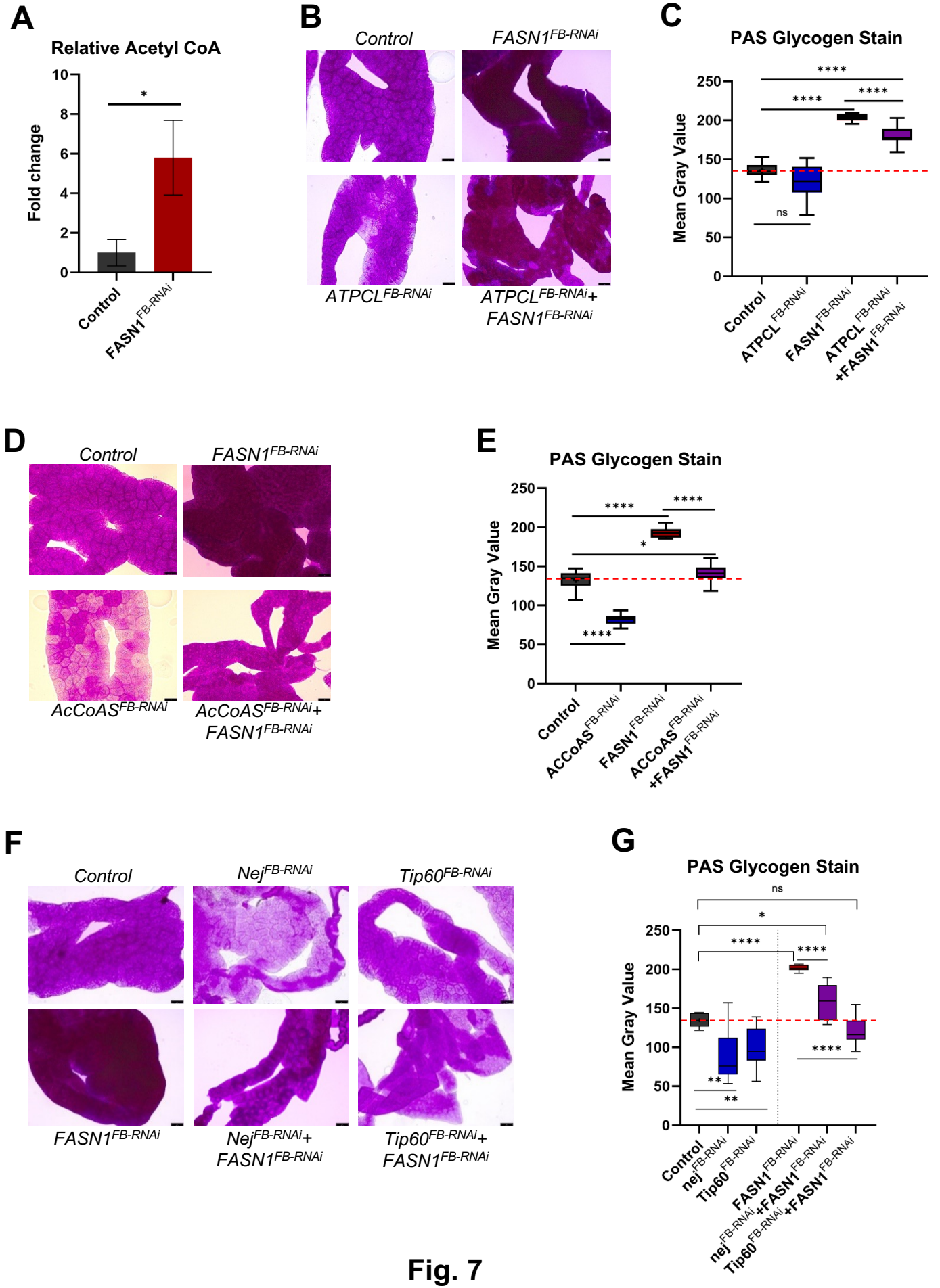
A
Relative Acetyl CoA
Fold change
10
8
6
4
2
0
*
Control
FASN1FB-RNAi
B
Control
FASN1FB-RNAi
ATPCLFB-RNAi
ATPCLFB-RNAi+
FASN1FB-RNAi
C
PAS Glycogen Stain
Mean Gray Value
250
200
150
100
50
0
****
****
****
ns
Control
ATPCLFB-RNAi
FASN1FB-RNAi
ATPCLFB-RNAi
+FASN1FB-RNAi
D
Control
FASN1FB-RNAi
AcCoASFB-RNAi
AcCoASFB-RNAi+
FASN1FB-RNAi
E
PAS Glycogen Stain
Mean Gray Value
250
200
150
100
50
0
****
****
*
****
Control
ACCoASFB-RNAi
FASN1FB-RNAi
ACCoASFB-RNAi
+FASN1FB-RNAi
F
Control
NejFB-RNAi
Tip60FB-RNAi
FASN1FB-RNAi
NejFB-RNAi+
FASN1FB-RNAi
Tip60FB-RNAi+
FASN1FB-RNAi
G
PAS Glycogen Stain
Mean Gray Value
250
200
150
100
50
0
ns
*
****
****
****
**
**
Control
nejFB-RNAi
Tip60FB-RNAi
FASN1FB-RNAi
nejFB-RNAi+FASN1FB-RNAi
Tip60FB-RNAi+FASN1FB-RNAi

Fig. 7

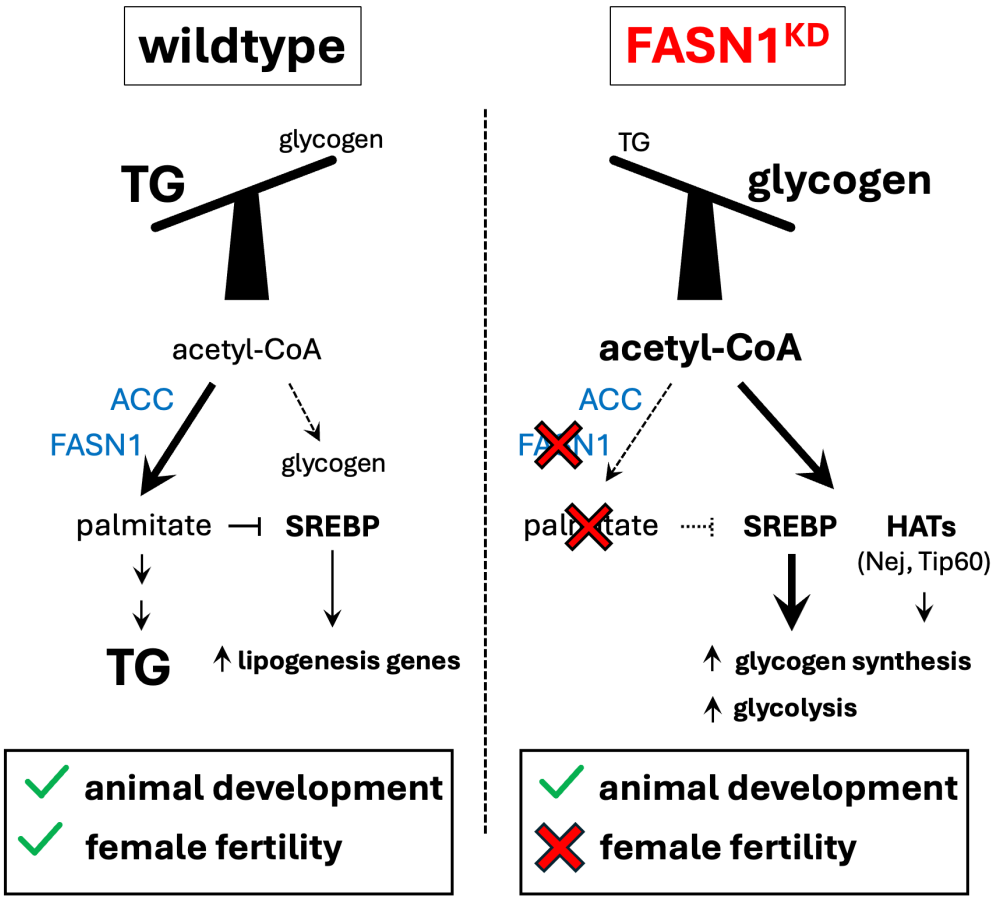
wildtype
FASN1KD
TG
glycogen
acetyl-CoA
ACC
FASN1
glycogen
palmitate
SREBP
TG
lipogenesis genes
animal development
female fertility
TG
glycogen
acetyl-CoA
ACC
FASN1
palmitate
SREBP
HATs
(Nej, Tip60)
glycogen synthesis
glycolysis
animal development
female fertility

Fig. 8